Spring 5-16-2014

Reducing Vortex-Induced Vibration of Drilling Risers with Marine Fairing

Aswin Janardhanan
University of New Orleans, ajanardh@uno.edu

Reducing Vortex-Induced Vibration of Drilling Risers with Marine Fairing

A Thesis

Submitted to the Graduate Faculty of the
University of New Orleans
In partial fulfillment of the
requirements for the degree of

Master of Science
in Engineering
Naval Architecture & Marine Engineering

By

Aswin Janardhanan

Bachelor of Technology, Cochin University of Science and Technology, 2008

May 2014

Dedicated to
my mother, Sheena & my brother, Aravind

Acknowledgement

Firstly, I thank Dr. Lothar Birk, my advisor, who through his magnificent character and experience, guided me throughout my thesis and master's program. Secondly, I would like to extend my gratitude towards Dr. Vimal Vinayan, Houston Offshore Engineering Inc, for his selfless support to assist me in completing my thesis. I'd also like to thank Dr. Brandon Taravella & all other faculty members of NAME department, for giving me valuable support and advice.

I would like to thank my mother Sheena, my brother Aravind, and my mentor Srg. Capt K.I. Mathai for being the strong encouragement and constant motivation to pursue my dreams. I'd also like to thank my best friends Cyril, Kaala, Jibin, Sajid, & Reshma and my roommates Chris, Nandu, Abin & Feby for being there for me whenever it counted.

I would also like to thank all my friends at CUSAT and UNO who were always there for me. I'd also like to thank Dr. Dileep K. Krishnan & Mr. Sivadasan Idiyath who continue to be a great motivation in my career life.

All the students in the NAME department were like a family, hanging out in the NAME lab, helping out each other academically and personally; which was the best thing I love about being a student at School of Naval Architecture & Marine Engineering, UNO. My stay at the University of New Orleans was worth every effort put in, and I will treasure this experience as long as my memory allows me to.

Special Thanks:

- Society of Naval Architects & Marine Engineering to provide financial support by means of scholarship money, without which I wouldn't have survived this long.
- CD-Adapco, for providing me a costly full-license of the software Star-CCM+ for free to work on my thesis work.
- School of Naval Architecture & Marine Engineering, UNO for providing me a good computer with enough computational capability to complete my work.

Contents

List of Figures

List of Tables

Abbreviations

BOP	Blowout Preventer
CFD	Computational Fluid Dynamics
DES	Detached Eddy Simulations
DNS	Direct Numerical Simulations
EIE	Extraneously-Induced Vibrations
IIE	Instability-Induced Vibrations
LES	Large Eddy Simulations
MIE	Movement-Induced Vibrations
RANS	Reynolds Averaged Navier-Stoke
TLP	Tension Leg Platforms
VIV	Vortex-Induced Vibrations

Notations

A	Reference area, m^2
A'	Added mass, kg
B	Damping of the system, N-s/m
C_D	Coefficient of drag
C_L	Coefficient of lift
C_y	Coefficient of force in y-direction
D	Diameter of the cylinder, m
E_{ij}	Mean rate of deformation tensor
F_D	Drag force, N
F_L	Lift force, N
$F_y(t)$	Excitation force in y-direction, N
$F_{x-viscous}$	x-component of viscous force, N
$F_{y-viscous}$	y-component of viscous force, N
$F_{z-viscous}$	z-component of viscous force, N
K	Mean kinetic energy, N-m/kg
L	Length of the body, m
M	Mach number
P	Absolute pressure, Pa
Re	Reynolds number
S	Mean strain rate tensor
S_t	Strouhal number
T_t	Reynolds tensor
U	Flow velocity, m/s
V_s	Velocity of light, m/s
a_{x-body}	x-component of body acceleration, m/s^2
a_{y-body}	y-component of body acceleration, m/s^2
a_{z-body}	z-component of body acceleration, m/s^2
e'_{ij}	Fluctuating component of deformation tensor
f_v	Vortex shedding frequency, Hz
k	Turbulent kinetic energy per unit mass, N-m/kg

k	Spring constant, N/m
m	Mass of the body, kg
u	x-component of velocity
v	y-component of velocity
v_b	Velocity of the body, m/s
w	z-component of velocity
x_0	Amplitude of vibration, m
μ	Dynamic viscosity, N-s/m^2
μ_t	Turbulent viscosity, m^2/s
ν_t	Turbulent kinematic viscosity, m^2/s
ω	Specific dissipation rate, /s
ω_n	Natural circular frequency, rad/s
ρ	Density of the fluid, kg/m^3
ε	Dissipation rate, m^2/s^3

Abstract

Since the offshore drilling for oil and gas is venturing into ever greater water depths, drilling risers face problems of vortex-induced vibrations due to the currents. Vortex-induced vibrations are a major fluid load and fatigue component on the long, smooth, and slender bodies placed in a fluid flow and measures must be taken to suppress the shedding of the Karman vortex sheets from its edges. One of the ways to reduce the vibration is to use marine fairings which are attached to the drilling risers with the help of weather vanes. In this thesis, CFD analysis based on solving RANS equations for K-ω turbulence model at Reynolds number 1.0×10^4 is done for a regular cylinder and one with marine fairing attached. The motivation of such analysis is to compute the efficiency of the fairing arrangement in suppressing the vortex-induced vibrations of the corresponding bluff body.

Keywords :

- CFD Simulation
- VIV Suppression
- Star CCM+
- Drilling Risers
- Marine Fairings

1 Introduction

1.1 Drilling Risers

Due to the huge rise in the demand for hydrocarbons, development of offshore oilfields has been growing fast over the past century. The risers used in offshore oil well drilling extend upto several thousand meters from the drilling vessel to the BOP. Floating or fixed structures are designed in order to maintain a prolonged offshore operation for a large period of time starting from a few months to several decades. A drilling riser can be defined as a conduit that provides a temporary extension of a subsea oil well to a surface drilling facility. Drilling risers can be categorized as either marine drilling risers used with a blow out preventer (BOP) on the ocean floor and generally deployed from floating drilling vessels, or tie back drilling risers used with a surface BOP installed topside on a fixed or very stable floating (like SPAR or TLP) platforms. The cross section of drilling risers are mostly bluff and circular.

1.2 Vortex-Induced Vibrations

The long span of drilling risers in the seawater is exposed to the flow-induced vibrations imparted by the ocean current. The flow around a drilling riser in ocean can be modeled as the external flow around a cylinder. Due to the pressure differences around the cylindrical body, vortices formed in the viscous boundary layer tend to detach at the downstream end of the cylinder causing the cylinder to oscillate in the direction normal to the flow. The oscillation of the structure caused by this entire flow instability is known as vortex-induced vibrations (VIV).

The frequency at which the vortices detach from the cylinder is called vortex shedding frequency. If it approaches the natural frequency of the cylinder resonance occurs thereby increasing the amplitude of the oscillations. This phenomena is called lock-in or synchronization. Vortex-induced vibration is a major issue faced by slender bodies in the field of ocean engineering, since they expose the bodies to cyclic stresses. Risers are arranged adjacently and once they start oscillating, there are high chances of collision with each other. The columns of floating structures like semi-submersibles, TLPs, SPARs, and the pipelines, risers etc all face the concern of VIV.

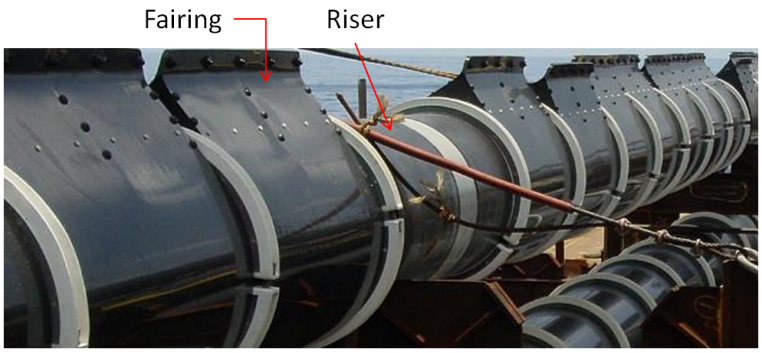

Figure 1.1: Marine fairings attached to the drilling risers [1]

The measure of adversity of VIV can be done by looking at two different variables

- amplitude of the oscillation and
- mean Drag Force

1.3 Marine Fairings

VIV induces an increase in the drag force on the drilling risers and thus reduces its fatigue life. So, it is highly advised to take measures to suppress the shedding of Karman vortex sheets [9] from the transverse edges of the cylinder. Usually for land-based structures, helical strakes are used to achieve this goal. But attaching helical strakes to long spans of drilling risers is impracticable due to high construction costs associated with it. An alternative option is to attach an appendage at the trailing end of the cylinder which is called a marine fairings. Usually marine fairings will have a weather-vane system that changes the direction of the fairings based on the flow in such a way that the fairings always remain at the trailing edge of the cylinder. The figure 1.1 shows a drilling riser fitted with marine fairings.

1.4 Computational Fluid Dynamics

Physical experiments in the field of fluid mechanics date back a couple of centuries. As more advanced mathematical theories were developed over the past few centuries, physical understanding of the fluid domain has increased. However, the mathematical theories are so complex that solution of the fluid flow using those theories has been impossible. But in the last century, with the introduction of computers, numerical analysis became available. This enabled researchers to use numerical methods

to supplement traditional physical model testing. This helped in understanding the problems where xperimental setups are too costly or tough to obtain reliable results. The availability of fast computing facilities has largely helped the research community in using computational fluid dynamics to solve and understand the fluid flow interior and exterior to the structure. Computational Fluid Dynamics (CFD) is nowadays regarded as one of the key elements in the design process of many systems in the marine industry.

Numerical simulations are a part of the active research work for offshore structures over the past few decades. Even though experiments are often preferred to obtain design data and verification, many offshore structures have huge aspect ratios which make it practically difficult to conduct scaled model testing. Model-testing is also constrained by factors such as experimental facility availability and capacity limitations, model scale limitations, difficulty in generating exact current profiles, costing and scheduling etc. With the introduction of CFD simulations, we have an exciting and cost-effective alternative for model tests.

1.5 Scope of Work

This thesis work includes the following:

- Familiarization with the concept of Flow-induced Vibrations
- Understanding the concept of Vortex-induced vibrations of a cylindrical structure
- Performing CFD simulations to calculate and application of methods to reduce VIV of bluff cylinders

1.6 Project Objectives

The main objectives of the thesis work include:

1. Understand the concept of VIV, its dependence on Reynolds number Re and bench marking of the CFD results with published experimental & computational results.
2. Understand the effectiveness of the fairing in suppressing the VIV of the cylinder.

1.7 Report Structure

The report structure will be organized in different chapters as given below:

- Chapter 1 : Introduction - provides basic introduction about the background of thesis
- Chapter 2 : Flow-Induced Vibrations - a brief description about the vibrations induced due to fluid flow
- Chapter 3 : Vortex-Induced Vibrations - a brief description about VIV
- Chapter 4 : Computational Fluid Dynamics - a brief description about history and application of CFD
- Chapter 5 : Bench-marking and Analysis Results - to illustrate the results obtained in this thesis work
- Chapter 6 : Conclusions and Recommendations from the completed thesis work - discussion about the results obtained and what to conclude from it. A small overview on the future works.
- Chapter 7 : References

2 | Flow-Induced Vibrations

2.1 Introduction

Flow-induced vibrations and fluid oscillations are usually approached using different descriptions by different disciplines that generally depend upon the structure type or the system involved. The occurrence of the flow-induced vibrations of structural and fluid masses occur in so many different forms that several volumes would be necessary to present them in terms of variety of possible structures or systems affected. It is really difficult to understand various vibrations, as the varying sources of excitation can take different forms and it makes the detection of the problem extremely difficult. It necessitates gathering information and experience from a structure and application of information to other structures, provided the basic ingredients of the excitation are well-identified.

2.2 Assessment of Flow-Induced Vibrations

Since the understanding of the flow-induced vibrations is hard, they are modeled using the basic elements [2] of:

- Body Oscillators
- Fluid Oscillators
- Sources of Excitation

Fluid modeling is very tenuous for arbitrary bluff structures. The fluid models thereby rely on non-linear extrapolations of the test measurements of lift, drag and surface pressure. Dynamic interactions of the structure and fluid models shall be then described using non-linear oscillation equations.

2.3 Body Oscillator

A body oscillator is an elastically supported rigid structure or structural part which can perform linear and angular movements or which is elastic to perform flexural movements. In other words, body oscillators are combinations of a mass and spring. Even the most simple systems might consist of a number of body oscillators each having a vibration problem by itself or in combination with other body or fluid oscillators. A body oscillator undergoes various different oscillations as given below:

- Free vibration

$$m\ddot{x} - B\dot{x} - Cx = 0 \tag{2.1}$$

- Forced vibration (harmonic and non-harmonic) Equation for the Harmonic vibrations are given by

$$(m + A)\ddot{x} - B\dot{x} - Cx = F(t) \tag{2.2}$$

- Self-excited vibration
- Parametrically excited vibration

2.3.1 Fluid loading response of body oscillators

1. **Effect of Viscosity** - The viscous effects on the fluid force exerted on a vibrating body in a stagnant fluid are described using a type of Reynolds number, $\omega_n D^2/\nu$, equivalent to the ratio of characteristic inertia and viscous forces. As the $\omega_n D^2/\nu$ value decreases, the fluid forces inserted by the flow will have increasingly higher damping and added mass components. The Reynolds number $\omega_n D^2/\nu$ must be greater than 5×10^3 if the inviscid result for the added mass A' from potential theory has to represent the added mass accurately on an unconfined cylinder in a viscous flow. When the cylinder is in a flow problem confined within wall boundaries, there is an increased added mass and damping.

2. **Effect of Amplitude** - The flow does not separate from the vibrating body as long as the vibration amplitude y_0 is small. For an unconfined circular cylinder of diameter D in a stagnant fluid, Sarpkaya [10] found that the separation of the boundary layer starts at $y_0/D = 0.2$, and vortex shedding starts at $y_0/D = 0.7$. When the vibration amplitude x_0 is larger than $0.7D$, the pattern of newly shed and old vortices of increasing complexity becomes more visible. When the vibrating body is placed in a flowing fluid, there will be an entirely different fluid-structure interaction. There will be energy flow from the mean flow to the vibrating body, which induces self-sustained body vibrations either due to the flow instabilities (vortex shedding) or movement-induced flow processes (galloping).

   For extraneously-induced excitations, the mathematical formulation incorporates either both the fluid added mass and fluid damping or fluid added mass

only as constant magnitudes in the 'structural components' of the equation of motion. The exciting force $F(t)$ is then purely flow-induced.
Parkinson [2], along with several other scientists, advocate a more rigorous approach where the 'structural components' of the equation of motion are separated from the 'fluid components'. The mass m and the damping B in the equation of motion should be interpreted as referring to the structure alone and the entire fluid-flow action on the body and its dependence on the body motion $y(t)$ should be described by fluid force.

$$m\frac{d^2y}{dt^2} + B\frac{dy}{dt} + Cy = F_y(t) \tag{2.3}$$

where, the excitation force $F(t)$ is given as:
for three dimensional bodies

$$F_y(t) = \frac{C_y L D \rho U^2}{2} \tag{2.4}$$

for two dimensional shapes

$$F_y(t) = \frac{C_y D \rho U^2}{2} \tag{2.5}$$

Sarpkaya [10] suggested the decomposition of the force coefficient C_y into two parts - one in phase with the body accelerations and the other in phase with the body velocity.

$$C_y = +C_m sin\omega_n t - C_d cos\omega_n t \tag{2.6}$$

$$C_m = 2y_{os}\omega_n^2 A'/\rho D U^2, C_d = 2y_{os}\omega_n A'/\rho D U^2 \tag{2.7}$$

The major distinction between cases with and without mean flow of the ambient fluid is the fact that A' and B are not constant for system with a given geometry, but instead functions of parameters describing the mean flow and the movement of the system such as:

- Geometrical conditions and roughness of the flow boundaries
- In-flow conditions, including background turbulence
- Flow parameters accounting for possible effects due to viscosity, gravity, surface tension, compressibility, vapor pressure etc

- Inertia, damping and stiffness properties of the body oscillator or, in case of controlled vibration, the frequency $f_s = \omega_n/2\pi$ and amplitude y_{os} of the vibration.

2.4 Fluid Oscillator

Fluid oscillators consist of a passive mass of the fluid which may undergo oscillations governed by fluid compressibility or gravity. A fluid-flow system consists of several number of fluid oscillators which may induce undesirable fluid pulsation when excited, and shall amplify the vibrations of a body oscillator if one of the natural frequencies coincide with the natural body oscillator frequency. Fluid oscillators are vital for the study of flow-induced vibrations for two major reasons:

- In a fluid-flow system, there will be fluid oscillations even without the presence of a body in it.
- A further enhancement of flow-induced vibrations of the body oscillator occur due to the fluid oscillators, most predominantly when one of their frequencies coincides with the natural frequency of the body oscillator or the dominant flow-instability frequency or both.

2.5 Sources of Excitation

There are different sources of excitation for body and fluid oscillators. Unfortunately they are difficult to detect. Table 2.1 provides an overview of the sources of excitations which are briefly explained below:

The basic frame work for classifying of the excitation is explained below:

2.5.1 Extraneously Induced Excitation (EIE)

EIE are caused by fluctuations in the flow velocity or pressure and independent of any flow instability originating from the body. Thus they are independent of structural movements except for added mass and fluid-damping effects. In most cases the exciting force is random, but may be periodic. The best examples for this case are bluff bodies being buffeted by turbulence of the oncoming flow and the pipe filled with compressible fluid exited by a loudspeaker. The most common sources of EIEs are:

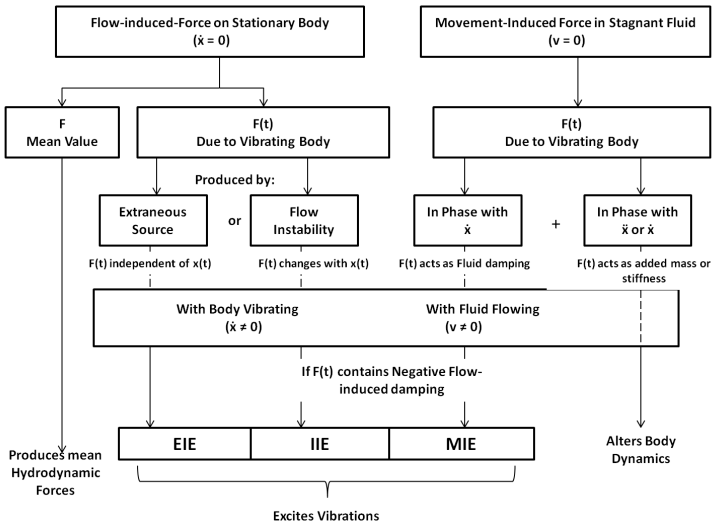

Figure 2.1: Schematics of forces exerted on a body by the surrounding fluid [2]

- turbulence (random)
- cavitation and some aspects of 2-phase flows (random/harmonic)
- oscillating flows including waves (random)
- earthquakes (random)
- machines and machine parts (random/harmonic)

2.5.2 Instability Induced Excitation (IIE)

IIE is the consequences of flow instabilities caused by the presence of a body in the flow that give rise to flow fluctuations, when a certain threshold value of flow velocity is exceeded. Perfect examples for this situation are the alternating vortex shedding from a cylindrical structure and the oscillations of an impinging free shear layer near the mouth of an organ pipe. The flow instabilities take the form of local instabilities producing the excitation forces even when there are no body or fluid oscillators present in the system. Therefore, this mechanism of excitation can be described in terms of a self-excited 'flow oscillator'. The type and strength of the control exerted on the flow instabilities play an important role in instability-induced vibrations of body or fluid oscillators. Such controls shall be fluid-dynamic, fluid-elastic or fluid-resonant in nature [2].

The excitation force in a fluid dynamic case, is the function of flow conditions only. The fluid-elastic and fluid-resonant cases have both the flow and resonating fluid oscillator defining the exciting force. A major feature in the fluid-elastic and fluid-resonant control is a lock-in of its frequency to that of the resonator within a certain range of flow velocities, thereby causing an amplification of the exciting force.
As there are large varieties of flow instabilities, researchers have constructed a minimum framework to differentiate them into the following groups:

- vortex shedding
- imping shear layers
- interface instabilities
- bistable-flow instabilities
- swirling-flow instability

2.5.3 Movement Induced Excitation (MIE)

The movement of the vibrating body or the fluid oscillator will generate a fluctuating force which causes an excitation. This is called movement-induced excitation. In the cases of EIE and IIE, excitation can be identified by examination of the flow without considering body motion, but in the case of MIE it is inherently linked to body movements and disappears if the body comes to rest. Whenever there is a body accelerating in the fluid, an alteration of the fluid forces on the body occurs due to the induced unsteady flow. If this alteration of the forces leads to a negative damping or to transfer of energy to the moving body, a self-excited body vibration is possible which is referred to as MIE.
The problem with MIE is that it cannot be detected from model tests unless the study is based on the anticipation of such occurrence and the tests based on that presumption. Furthermore, MIEs can be simulated if significant parts of the structure are reproduced with similar mass, damping and elastic characteristics.
MIEs can be classified into four main divisions

1. **MIEs independent of coupling** - Primary feature of this type of MIE is that the motion of a single body in a single mode suffices to change the fluid forces in a way that energy is transferred from the flow to the moving body. In

cases like galloping, the exciting force can be described in a more or less quasi-steady manner, while the cases of stall flutter energy transfer and excitation is brought about by the deviation from the quasi-steadiness.

2. **MIEs involving coupling with fluid-flow pulsations** - This type of MIE can be identified by the pulsation in discharge and/or head that arises in conjunction with the body oscillation. If the fluid-inertia forces accompanying the discharge variations are likely to act in the direction of body velocity, energy will be transferred to the body and the necessary condition for MIE will be satisfied.

3. **MIEs with mode coupling** - This type of MIE involves simultaneous movements of a body in two or more modes. Each mode may be independently free of MIE, but vibration in another mode will be capable of producing fluid forces which will transfer flow energy to the body in other mode(s). Frequency-merging is also a resultant of this type of MIE, that is the frequency of each mode must be a function of flow velocity such that two of them merge to a common value at a certain velocity.

4. **MIEs with multiple-body coupling** - The motions of neighboring bodies influences one another through fluid-dynamic coupling which plays an essential role in the excitation.

The above classification involves sharp lines of demarcation between one another as such classifications may be inappropriate in many different cases. Furthermore, there is a big amount of risk involved in codifying existing knowledge at a time when the state of understanding is as incomplete as it is on this subject. For this reason, the classifications must be treated as a mere preliminary tool for organizing the assessment of flow-induced vibrations in engineering systems rather than a standard structure for classifying flow-induced vibrations. A brief description of sources of excitation based on either body oscillator or fluid oscillator is given in the Figure 2.2.

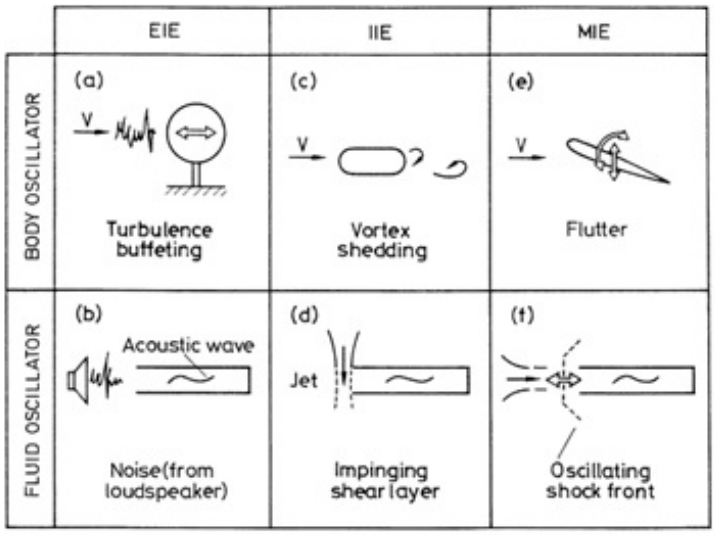

Figure 2.2: Examples of fluid & body oscillators under various excitations [2]

This thesis report is focused on vortex-induced vibration of cylindrical structures, which are a result of flow instabilities due to the presence of a body. So, it is a classic example for instability-induced vibrations.

2.6 Non Dimensional Numbers in Fluid Dynamics

2.6.1 Reynolds Number

The Reynolds number Re is a ratio of inertial forces and viscous forces. It is useful in quantifying the relative importance of these two types of forces in any given flow.

$$Re = \frac{\rho U D}{\mu} \tag{2.8}$$

Small Re indicate the flow is viscous dominant. Small Re is also associated with laminar flow field. If the flow is inertial dominant we will have high Reynolds numbers indicating a turbulent flow. The effect of turbulence is explained further in Chapter 4.

2.6.2 Strouhal Number

Strouhal number is useful in describing oscillating flow mechanisms.

$$S_t = \frac{f_v D}{U} \tag{2.9}$$

where,
f_v is the vortex shedding frequency,
D is the diameter of the bluff cylinder,
U is the mean flow velocity

3 | Vortex-Induced Vibrations

3.1 Introduction

Among all the flow instabilities so far under the consideration in various research projects, wakes past bluff cylindrical bodies have received by far the greatest attention. Vibrations induced by the periodic shedding of vortices are those that most frequently occur in engineering practice. Vortex-induced vibrations are a classic example of instability-induced vibrations. At very low Reynolds numbers, potential flow theory can be utilized perfectly to explain the flow around a bluff cylinder. But with the increase of the Reynolds number, boundary layers detach from the sides of the cylinder, and potential theory is no longer valid. This can be explained on the basis of formation of boundary layers of fluid around the body, wherever viscous forces occur in the layer of fluid close to the solid surface and flow separation of the boundary layers [9].

3.2 Vortex Shedding

When a bluff cylinder is placed in a flow, shear layers are formed due to the separation of the boundary layer around the cylinder. As the shear layer moves away from the cylinder, its strength increases and further grows until a stronger shear layer breaks off the former shear layer. This results in vortex shedding. A repeated process of the detachment results in a Von Karman Vortex Street. The behavior of the vortex shedding can be defined using the Strouhal number, which is the non-dimensionalized form of the vortex-shedding frequency.

3.3 Principle Behind Vortex-Induced Vibrations

As the flow of the fluid approaches the upstream edge of the bluff cylinder, the pressure in the fluid particle rises from the free stream pressure value to the stagnation pressure. The high fluid pressure impels the developing boundary layers along both sides of the cylinder, but as the flow approaches the downstream end the pressure values are inadequate to force the boundary layers around the cylinder anymore. Closer to the transversely widest section of the bluff cylinder, the boundary layers separate from each side of the cylinder surface forming two shear layers that trail behind the cylinder in the flow. The free shear layers bound the wake of the flow. The outer end of the shear layer gets detached from the cylinder fast, while the inner

end of the layer is shed last and tends to move slower than the outer end which is already in contact with the free streams. This causes the shear layer to roll into discrete swirling vortices.

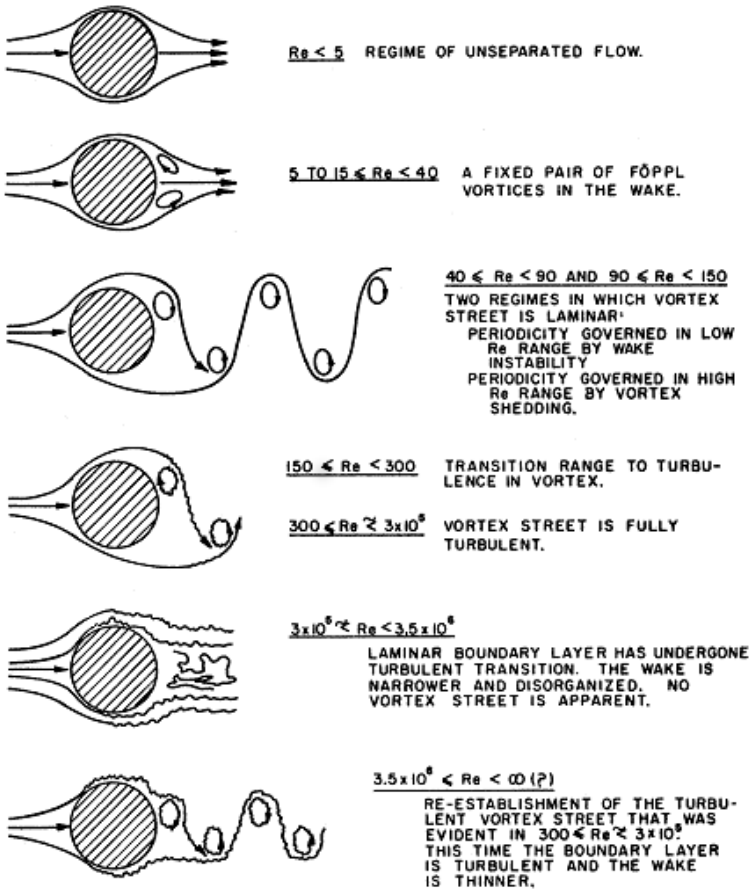

Figure 3.1: Fluid flow regimes across circular cylinders [3]

3.4 Flow Regime

Possible fluid flow regimes across the circular cylinders are given in the Figure 3.1. As described in the Figure 3.1 at very low Reynolds number, $Re < 5$, inertia effects are negligible and the pressure recovery at the downstream end of the cylinder is almost complete. Thus, the flow is properly represented by potential flow theory at these Re values. Vortex shedding does not occur. As the Reynolds number Re is increased, a pair of fixed vortices is formed immediately behind the cylinder. When

Re is further increased, the vortices elongate until one of the vortices breaks away and a periodic wake and staggered vortex street is formed. The vortex street is laminar up to Re values of 150, and becomes turbulent above Re values of 300. Then the vortex street degenerates into a fully turbulent flow beyond approximately 50 diameters downstream of the cylinder. Re values in the range of 300 to 3×10^5 is called subcritical range, since it's occurrence is prior to the onset of the turbulent boundary layer at Re of 3×10^5. The vortex street is however turbulent and occurs at a well defined frequency for subcritical range. At the laminar-turbulent transition, flow separation happens at a more downstream point of the cylinder. Shedding of vortices becomes disorganized and the drag drops sharply (see Figure 3.2). At higher supercritical values of the $Re > 3 \times 10^5$, boundary layer becomes turbulent and the vortex street is reinstated [9, 11, 10, 12].

3.5 Drag & Lift Forces

Due to the periodical change in the pressure distribution on the cylinder surface, force components on the cylinder will also vary periodically. The force components on a cylinder in a flow can be subdivided into a drag force which is the in-line with the flow direction and the lift force which acts in the cross-flow direction.

The drag and lift force coefficients are given by:

$$C_D = \frac{F_D}{\frac{1}{2}\rho A U^2} \tag{3.1}$$

$$C_L = \frac{F_L}{\frac{1}{2}\rho A U^2} \tag{3.2}$$

where, A = reference area U = flow velocity

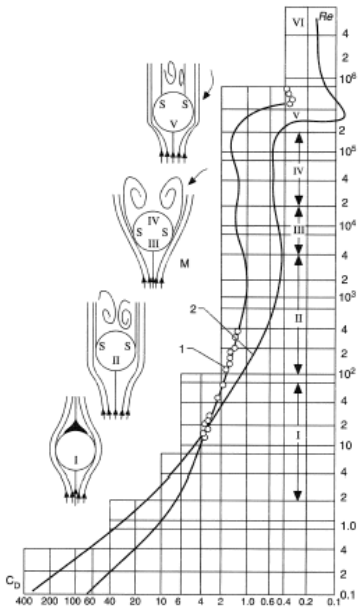

Figure 3.2: Drag Coefficient vs Reynolds Number [4]

3.6 Methods to reduce Vortex-Induced Vibrations

Reduction of VIV amplitudes can be achieved using different ways. In this section the most important ones are outlined:

3.6.1 Increasing Structural Damping

The resonant vibrations of the cylinder will gradually diminish if the mass or structural damping of the cylinder can be considerably increased. Damping can be increased by various means, such as [3]:

- Permit scraping between structural elements
- Use of composite materials like concrete instead of welded steel
- Incorporate materials with high internal damping such as wood, rubber, sand, etc.
- Use of external dampers

3.6.2 Avoiding Resonance

If we make sure the natural frequency does not coincide with the vortex shedding frequency of the structure, VIV can be suppressed. This can be obtained by increas-

ing the stiffness of the structure using wires or braces, which is ordinarily impractical solution when it comes to large or complex structures.

3.6.3 Suppression Devices

Suppression devices are attachments to the cylinder which assist in reducing the VIV. M.M. Zdravkovich [5] compiled the suppression devices into three major groups:

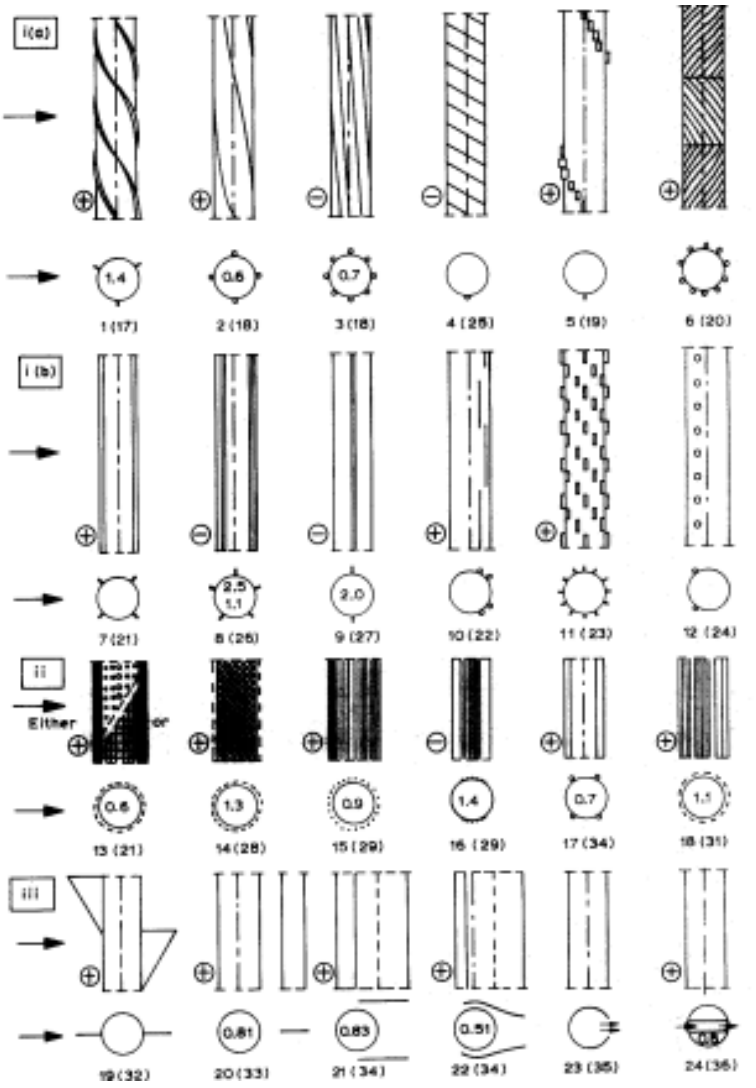

Figure 3.3: Aerodynamic & hydrodynamic means for interfering with vortex shedding [5]

3.6.3.1 Surface Protusions

They affect the separation lines and/or separated shear layers. The best examples of this are strakes, wires, fins, studs etc. They are further subdivided into representative types:

1. **Omni-Directional Devices** - As the word 'omni-directional' indicates, they don't have a preferred direction. Helical strakes are examples of an omni-directional device to suppress VIV.

2. **Uni-Directional Devices** - These devices have an optimal direction at which they are very effective and less effective at others.

3.6.3.2 Shrouds

They affect the entrainment layers. The best examples of this are gauze, perforated rods, axial rods and axial slats etc. These devices run completely around the cylinder. Marine fairings fall into this category.

3.6.3.3 Nearwake Stabilizer

The best examples of are splitter plates, saw-tooth plates, guiding plates, vanes, base-bleed, slits cut along the cylinder etc.

4 | Computational Fluid Dynamics

4.1 Introduction

Fluid dynamics is the science of fluid motion. Usually we employ three different methods to study the fluid motion:

1. Experimental fluid dynamics
2. Theoretical fluid dynamics
3. Numerical fluid dynamics, also known as Computational Fluid Dynamics (CFD)

Computational fluid dynamics (CFD) is defined as the science of predicting fluid flow, heat transfer, mass transfer, chemical reactions, and related phenomena by solving the mathematical equations which govern these processes using a numerical solver. A brief history of fluid mechanics and CFD are provided in the Figure 4.1 & Figure 4.2.

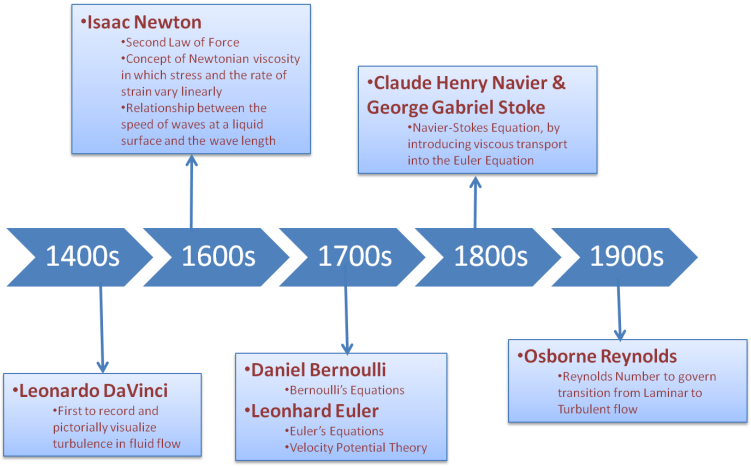

Figure 4.1: Timeline of fluid mechanics developments before 20th century

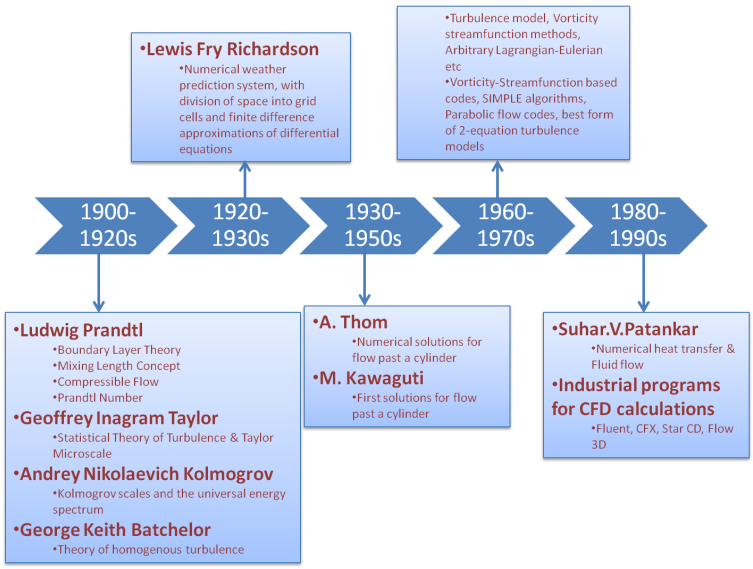

Figure 4.2: Timeline of fluid mechanics developments in 20th century

4.2 Working of Computational Fluid Dynamics

The process of CFD analysis can be broken down into the following steps:

- An analysis in CFD begins with the mathematical modeling of the physical problem.
- The solution domain must be defined based on area of focus.
- Discretization of the flow field and the body of interest to develop approximations of the governing fluid mechanics in the fluid region of interest. The discretization splits the body of interest into nodes and cells and set of algebraic equations are numerically solved for the flow field variables at each node or cell.
- Fluid properties are modeled.
- Basic assumptions are made to simplify the problem (e.g. steady state flow, incompressibility, inviscid, two-dimensional flows)
- Define appropriate initial and boundary conditions for the problem.
- A numerical solver must be selected based on which the computations are done.

- All the conservation theories including conservation of mass, momentum and energy must be satisfied throughout the region of interest.
- Post-processing of the solutions are done to extract quantities of interest (e.g. lift, drag, torque, heat transfer, separation, pressure loss etc.)

A visual breakdown of the CFD simulation schematics is provided in the figure 4.3

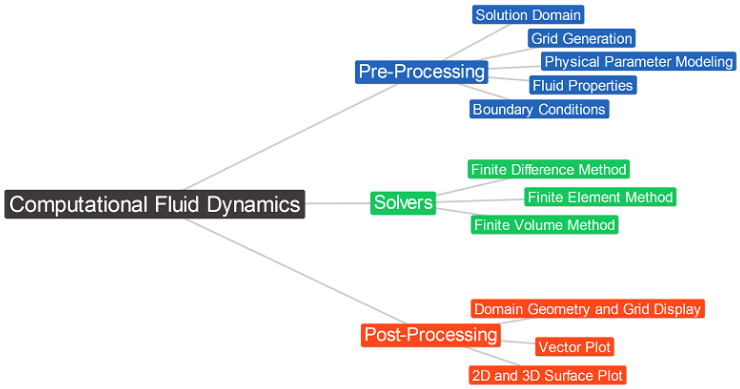

Figure 4.3: Schematic breakdown chart for CFD simulation [6]

4.3 Conservation laws of fluid motion

CFD problems are defined using a set of mathematical equations based on conservation of mass, momentum and energy. As in case of external flow problem at subsonic speeds, the conservation of energy is assumed to be satisfied, and therefore is based on conservation of mass and momentum only.

4.3.1 Conservation of mass

For any system which is closed to all transfers of matter and energy, the mass must remain constant over the time since no mass or added or removed from the system. Therefore the mass of the system is conserved.

$$\iiint_V \frac{\partial \rho}{\partial t} dV = - \iint_S \rho \overline{u} \cdot \overline{n} dS \tag{4.1}$$

4.3.2 Conservation of momentum

By applying Newton's second law in a fluid domain, Claude-Louis Navier and George Gabriel Stokes [7] derived the conservation of momentum equation. This defines that

any change in the momentum of a fluid within a control volume will be due to the net flow of the fluid into the control volume and the external forces acting on the system. For an incompressible fluid this results in:

$$\iiint_V \frac{\partial \rho u}{\partial t} dV + \iint_S (p\bar{i} + \rho u \overline{V}) \cdot dS = \iiint_V \rho a_{x-body} dV + F_{x-Viscous} \tag{4.2}$$

$$\iiint_V \frac{\partial \rho v}{\partial t} dV + \iint_S (p\bar{j} + \rho v \overline{V}) \cdot dS = \iiint_V \rho a_{y-body} dV + F_{y-Viscous} \tag{4.3}$$

$$\iiint_V \frac{\partial \rho w}{\partial t} dV + \iint_S (p\bar{k} + \rho w \overline{V}) \cdot dS = \iiint_V \rho a_{z-body} dV + F_{z-Viscous} \tag{4.4}$$

4.4 Meshing strategies

Figure 4.4 shows two basic meshing strategies, which are briefly explained below:

4.4.1 Structured Meshes

Structured meshes are computationally less intensive and can be used in cases with simple geometry. The grid lines pass all through domain. It operates by sweeping a surface mesh from the surface of a CAD geometry through its volume [7].

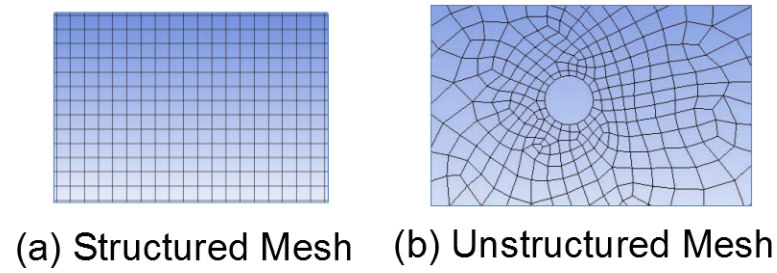

Figure 4.4: Basic meshing strategies [6]

4.4.2 Unstructured Meshes

In an unstructured mesh type, the cells are arranged in an arbitrary fashion and there are no directional constraints on the cell layout. Analysis for domains with

unstructured meshes will take more CPU time, as solving the linearized equations becomes more difficult.

4.5 Boundary Conditions

Solving the Navier-Stokes equations require appropriate initial conditions and boundary conditions as they assist in specifying the fluxes into the computational domain. In short boundary conditions define the limits of our solution domain. A brief introduction about the different boundary conditions in a flow is given below:

1. **Inlet boundary condition** - permits the flow to enter the solution domain. An inlet can be a velocity, pressure or mass flow. In our case we have a fluid flow condition, so it is optimal to give a velocity inlet condition where the flow enters the domain in a constant velocity.

2. **Outlet boundary condition** - it permits the flow to exit the solution domain. Velocity, pressure or mass flow are specified. In our case, we define it as a pressure outlet.

3. **Wall boundary condition** - walls provide rigid limits to the solution domain. There will be no flow through the walls. For a body boundary we generally define a no-slip condition which means there will be a tangential component of shear stress towards the domain. The far field conditions are defined as slip which means zero-shear stress at the wall. There will be no reflection of the flow from these walls.

4. **Stagnation boundary condition** - this defines a uniform value across the boundary for either pressure or velocity.

4.6 Discretization Techniques

The fluid flow problem is solved with the help of various numerical techniques, which are in general known as discretization methods. The differential equations are approximated by a system of algebraic equations. Its solution provides values for the variables at a set of discrete location in space and time. There are three basic techniques, but where the grid is very fine, all these techniques would yield same solution even though they all approach the problem differently.

1. **Finite difference method** - This is the easiest to use and is mostly used for simple geometries. Although it can be applied for structured and unstructured

grids, it is more effective on structured grids. The method is inappropriate for complex geometries. Also special considerations have to be observed to achieve the conservation conditions.

2. **Finite element method** - In this method, the domain is broken into unstructured discrete volumes or finite elements. The unstructured grids will consist of triangles or quadrilaterals (2D) and tetrahedral or hexahedra (3D). Since we use an unstructured mesh, the matrices of linearized equations are not well ordered as that of a structured mesh. This makes solving the systems of algebraic equations less efficient.

3. **Finite volume method** - Finite volume method is the most common method used in CFD computations. Any type of grid can be used while implementing this method. In this method, the fluid domain is divided into a finite number of control volumes and the conservative equations are satisfied for each control volume. This method requires interpolations and integration, for higher order problems. This makes it highly difficult to work with in a 3D problem.

4.7 Turbulence

Turbulence is a flow regime which is characterized by random property changes including momentum diffusion, high momentum convection, and rapid variation of pressure and velocity in space and time. Most of the commonly found fluid flows such as jet streams, combustion, boundary layers over the wings of aircraft etc are turbulent in nature. The major trouble with turbulence is the difficulty to define it, but it has the following characteristics:

- **Irregular**: Turbulence is highly random in nature which makes a full deterministic approach to describe it very difficult. For that reason, turbulence is described statistically.

- **Diffusive**: Diffusion is the major cause for the rapid mixing and increased rates of momentum, heat and mass transfer. A flow cannot be concluded turbulent just because of the irregularity in it, while it can be described turbulent only because of its diffusive character.

- **Large Reynolds number**: Turbulence always occurs at high Reynolds numbers, when there is a complex interaction between the viscous terms and the inertia terms in the momentum equations.

- **Vorticity fluctuations**: Turbulence comes with a non-zero vorticity.
- **Dissipative**: Turbulence must be driven, otherwise it decays and the flow becomes laminar.
- **Continuum**: During turbulence, even the smallest eddies are significantly larger than the molecular scales, which makes it a continuum phenomenon. Therefore, it is governed by the equations of fluid mechanics.

When present, turbulence dominates all other flow phenomena and results in increased energy dissipation, mixing, heat transfer and drag. In one way, turbulence can be described as the ability of the flow to generate new vorticity from the existing vorticity [7].

Turbulence modeling is the use of a constructed model to predict the effects of turbulence. It can also be described as a computational procedure to close the system of mean flow equations. For most of the engineering problems, it is quite unnecessary to resolve the details of the turbulent fluctuations as we are largely interesting in studying the effect of turbulence on the mean flow. In other words, the objective of turbulence modeling is to develop equations that will predict the time-averaged velocity, pressure, and temperature fields without resolving the complete turbulent flow patterns as a function of space and time. Any given turbulence must have the following properties to be useful:

- wide applicability
- accuracy
- simplicity
- economical

4.7.1 Common Turbulence Models

Turbulence models are inexact representations of the physical phenomena which is being modeled and none of the turbulence models has any kind of superiority over the others in all flow simulations. So, it is advisable to provide a suite of models that reflect the current state of the art.

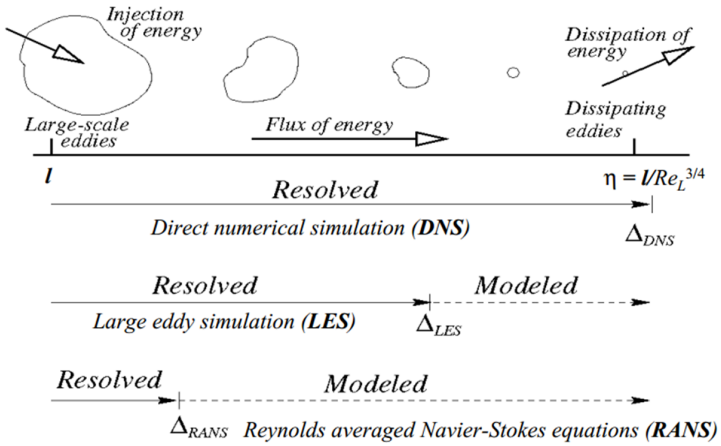

Figure 4.5: Different turbulence models [7]

4.7.1.1 Classical Models (Based on RANS Equations)

RANS equations are a simplified version of the complex Navier-Stokes equations for the instantaneous velocity and pressure fields which are decomposed into a mean value and a fluctuating component. The averaging process consists of time averaging for steady-state situations and ensemble averaging for repeatable transient situations. The resulting equations for the mean quantities are identical to the original equations, but with an additional term that appears in the momentum transport equation. The additional term is a tensor quantity called Reynolds stress tensor with the following definition:

$$T_t = -\rho \begin{bmatrix} \overline{u'u'} & \overline{u'v'} & \overline{u'w'} \\ \overline{u'v'} & \overline{v'v'} & \overline{v'w'} \\ \overline{u'w'} & \overline{v'w'} & \overline{w'w'} \end{bmatrix}$$

The Reynolds stress tensors have six independent components, $-\rho\overline{u'u'}$, $-\rho\overline{u'u'}$ & $-\rho\overline{u'u'}$ are the internal normal stress acting on the mean turbulent flow in x, y & z-directions respectively and the $-\rho\overline{u'v'}$, $-\rho\overline{u'w'}$ & $-\rho\overline{v'w'}$ are the shear stress tensors. The stress tensors must be symmetric to avoid local singularities in the rotational motion of the continuum. Major challenge in RANS equation based solutions is to model the Reynolds stress tensor T_t in terms of the mean flow quantities and hence provide a closure of the governing equations. The classical RANS equation based models can be subdivided into eddy viscosity models and stress transportation

models. We have further subdivisions under eddy viscosity models as mixing length model, Spalart-Allmaras model, k-ϵ model and k-ω model [7].

- **Eddy viscosity models** They work on the concept of turbulent viscosity μ_t, in order to model the Reynolds stress tensor as a function of mean flow quantities. The most basic model is known as the Boussinesq approximation:

$$T_t = 2\mu_t S(2/3)(\mu_t \nabla \mathrm{v} + \rho k)\mathbf{I} \tag{4.5}$$

  where,

$$S = 1/2(\nabla \mathrm{v} + \nabla \mathrm{v}^T) \tag{4.6}$$

  I is an identity matrix. The assumption that the Reynolds stress tensor is linearly proportional to the mean strain rate tensor (S) is known to be flawed. Some of the 2-equation based models include non-linear constitutive relations to extend the linear approximations.

  - **Zero equation or mixing length model:** Mixing length models are easy to implement and have shorter computation times. They provide a good precision for simple flows. However, they are incapable of describing flows where the turbulent length scale varies or if there is flow separation. Their computational capabilities are limited to mean flow properties and turbulent shear stress. They can be typically used for simple external aero flows.
  - **1-equation or Spalart-Almaras model:** Spalart-Almaras model solves a single conservative partial differential equation for turbulent viscosity, which contains convective diffusive transport terms, as well as expressions for the production and dissipation of turbulent viscosity. They are well versed in solving the flows with mild separation where the boundary layers are largely attached. They are incapable of modeling a massively separated flow, free shear flows or decaying turbulence.
  - **k-ε model (2-equation):** This model focuses on mechanism that affects the turbulent kinetic energy k and its dissipation rate ε.
    Instantaneous kinetic energy, k(t) = Mean kinetic energy K + turbulent kinetic energy k

If k and ϵ are known, we model the turbulent viscosity as

$$\nu_t \propto \mathrm{k}^2/\varepsilon \tag{4.7}$$

The equation for the mean flow kinetic energy K is given as:

Rate of change of K + convection transport of K =
pressure transport of K + viscous stress transport of K + Reynolds stress transport of K - dissipation rate of K - turbulence production

$$\frac{\partial(\rho \mathrm{K})}{\partial t} + div(\rho \mathrm{K} U) = div(-PU + 2\mu U E_{ij} - \rho U \overline{u_i' u_j'}) - 2\mu E_{ij} \cdot E_{ij} - (-\rho \overline{u_i' u_j'} \cdot E_{ij}) \tag{4.8}$$

The equation for turbulent kinetic energy k is given below:

Rate of change of k + convection transport of k =
pressure transport of k + viscous stress transport of k + Reynolds stress transport of k - dissipation rate of k - turbulence production

$$\frac{\partial(\rho \mathrm{k})}{\partial t} + div(\rho \mathrm{k} U) = div(-\overline{p' \mathrm{u}'} + 2\mu \overline{\mathrm{u}' e_{ij}'} - 0.5\rho \overline{u_i' . u_i' u_j'}) - 2\mu e_{ij}' \cdot e_{ij}' - (-\rho \overline{u_i' u_j'} \cdot E_{ij}) \tag{4.9}$$

A simplified equation for k is commonly used. We can obtain the model equations for dissipation rate ε by multiplying the equation for turbulent kinetic energy by $\frac{\varepsilon}{\mathrm{k}}$. Reynolds stresses are then calculated from k and ε.

k-ε models are relatively simple to implement leading to stable solutions. On one hand they are good enough for a reasonable prediction of the turbulence for fully developed turbulent flow. On the other hand they poorly predict swirling flows, rotating flows, and strongly separated flows. This model follows an incorrect assumption that all normal stresses are equal, leading to inaccuracy in results.

- **k-ω model (2-equation):** Is similar to the k-ε model. However it uses

specific dissipation rate ω over the dissipation rate ε.

$$\omega = \frac{\varepsilon}{\mathrm{k}} \tag{4.10}$$

Similar to k-ε model, this model solves two additional partial differential equations (PDEs):

* Modified version of k equation in the k-ε model
* Transport equation for ω

The turbulent viscosity is then calculated as :

$$\nu_t = \rho\frac{\mathrm{k}}{\omega} \tag{4.11}$$

One of the major advantages of this model is the improved performance for boundary layers under adverse pressure gradients. It can be applied without further modification throughout the boundary layer, including viscous-dominated regions.
However these models are not applicable to internal flows, as the boundary layer is sensitive to the omega values in the free streams. They have similar drawbacks as that of a k-ε model, such as the assumption of isotropic μ_t [7][13].

- **7-equation or Reynolds stress transport model:** They are also known as second-moment closure models and are amongst the most complex turbulence models. They are computationally expensive models. By solving transport equations for all components of the specific Reynolds stress tensor, they naturally account for the effects of anisotropy due to strong swirling motion, streamline curvature, rapid changes in strain rate and secondary flows in ducts. They are used when the turbulence is highly anisotropic, similar to that of swirling flow in a cyclone separator. Physically, they are the most complete models available and require more CPU effort due to the tightly coupled momentum and turbulence equations. Also, there is a penalty of total number of iterations required to obtain a converged solution.

4.7.2 Large Eddy Simulations

In Large Eddy Simulation (LES) models, large eddies are retained and small eddies removed. Small eddies are then modeled using a subgrid-scale model, while large

eddies are solved directly using a transient calculation. Since the modeling of turbulence is of lesser extent, the errors that might occur due to assumptions incorporated in the turbulence modeling are less consequential. The hypothesis that smaller eddies are self similar and thus lend themselves to simpler and more universal models. Thus, they are highly accurate compared to RANS equations based models, but less compared to Direct Numerical Simulation (DNS) models.
A disadvantage of this approach is its high computational expense. Necessary storage and analysis of large data sets is also a major impediment.

4.7.3 Detached Eddy Simulations

Detached Eddy Simulation (DES) is a hybrid model that combines the features of RANS simulation in some parts of the flow and LES in other parts. DES turbulence models are set up in such a way that the shear layers are solved using a basic RANS closure model. The turbulence model is however modified so that it will emulate a basic subgrid scale model, if the grid is fine enough. In this way a combination of advantages of RANS simulation in the shear layers and an LES simulation in the unsteady separated regions is obtained. They are highly recommended for flow separation problems due to their hybrid quality and is a more practical approach for vortex-shedding problems [13].

4.8 Errors in CFD

4.8.1 Modeling errors

This type of error is common in the RANS equation based turbulence models. It causes a difference between the numerically computed solution and the actual flow. The error can be reduced by comparing the results with the available experimental data or solutions obtained from better turbulence model.

4.8.2 Discretization errors

Discretization errors occurs when there are differences in the results due to changes in mesh sizing. This type of error can be reduced by checking the refinement extent of the mesh size and is proportional to the difference of solutions obtained on consecutive grids.

4.8.3 Iteration errors

This is the error between the iterative and exact solution of the system of algebraic equations. The error can be controlled by monitoring the amount of reduction of residual norms compared to initial values.

5 | Problem Description & Results

5.1 Description of the Problem

In this thesis, the author is studying the VIV of cylindrical structures and how VIV amplitude would differ once a fairing is attached to the downstream end of the cylinder. This study has two parts:

- Bench marking of the drag coefficients with respect to the available experimental data for regular cylinders at different Reynolds numbers (100, 500, 1000, & 10000)
- Study of VIV amplitudes of a regular cylinder (Configuration 1) and a cylinder with fairing attachment (Configuration 2)and compare the results

5.2 Configurations Considered as Oscillation Models

Two different configurations are studied and their transverse oscillation are compared. Figure 5.1 shows the two different configurations being studied.

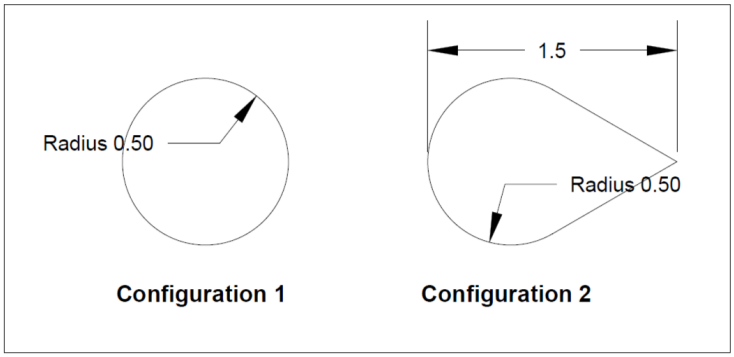

Figure 5.1: Geometry of Configurations

5.3 Bench-marking of the Drag Coefficients

The CFD analysis is conducted for a bluff cylinder at various Reynolds numbers and the drag coefficients are compared with the published experimental results.

5.3.1 Flow Separation

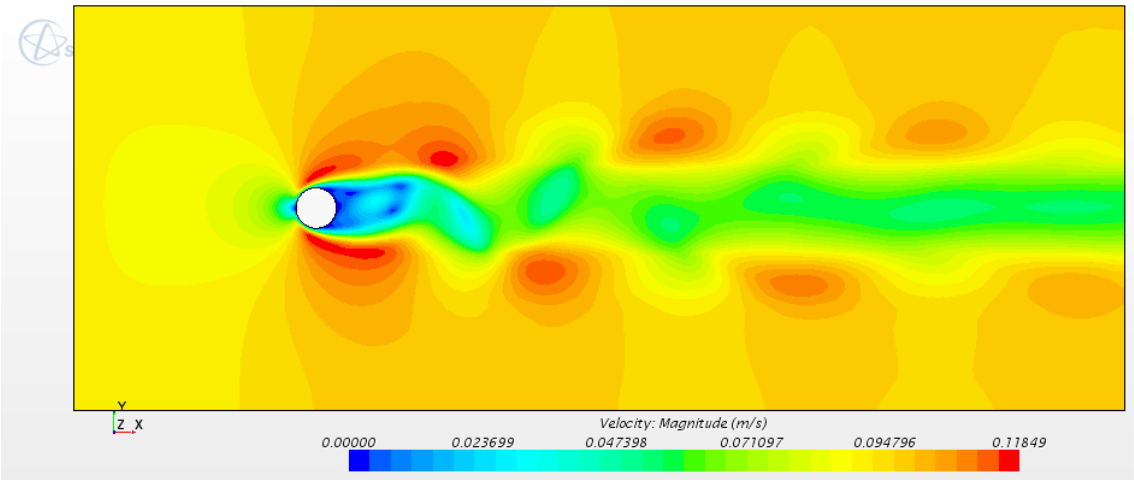

Figure 5.2: Flow separation and velocity distribution for $Re = 100$

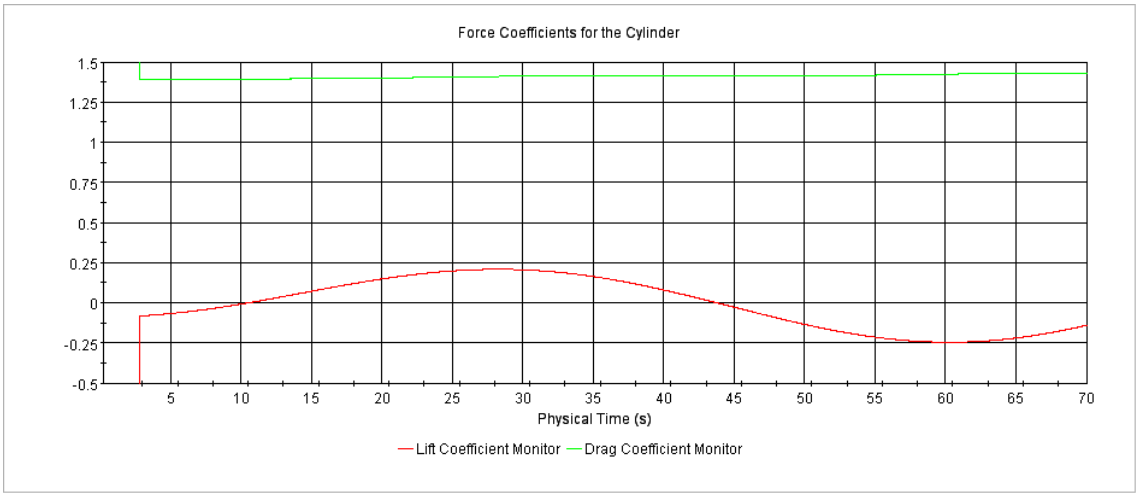

Figure 5.3: Solution history for lift and drag coefficients for $Re = 100$

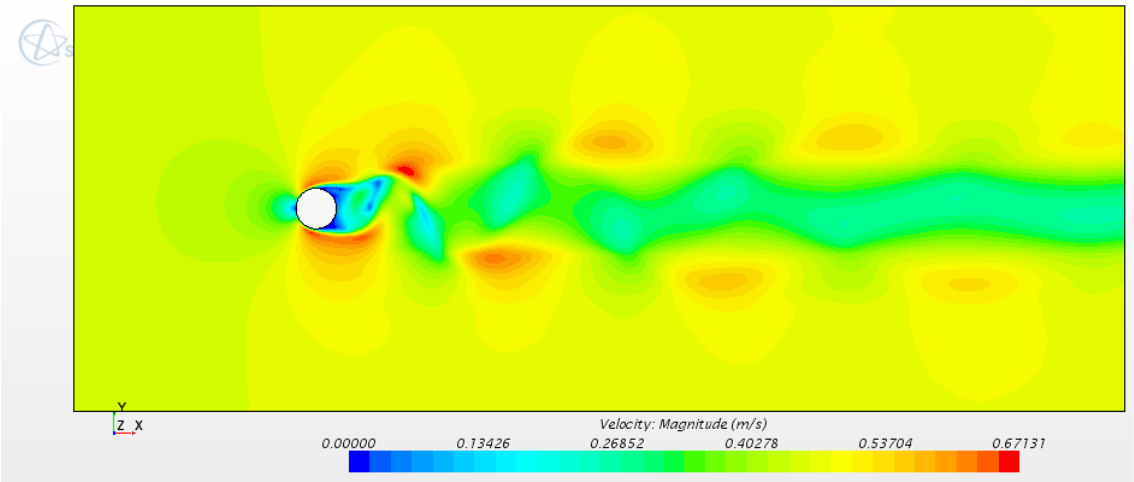

Figure 5.4: Flow separation and velocity distribution for $Re = 500$

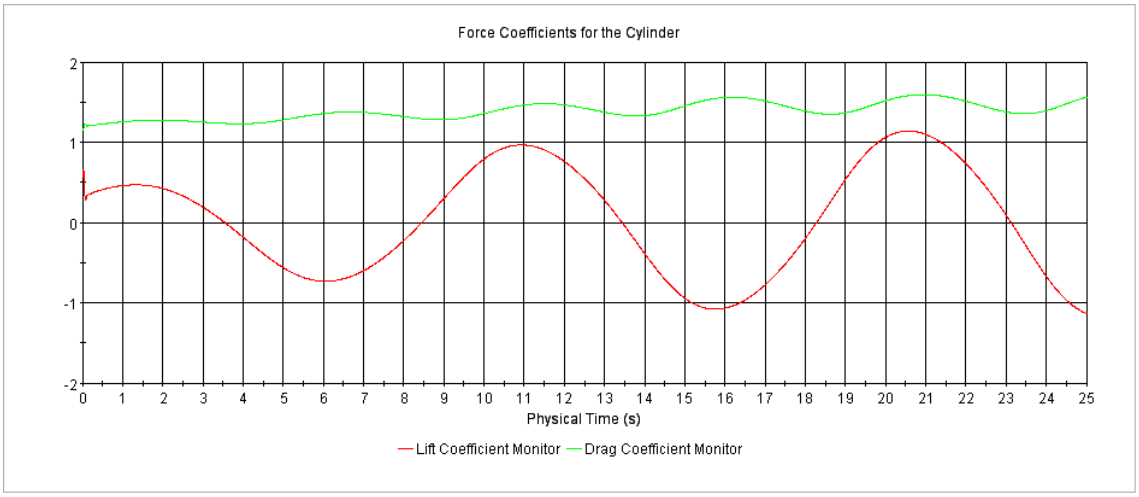

Figure 5.5: Solution history for lift and drag coefficients for $Re = 500$

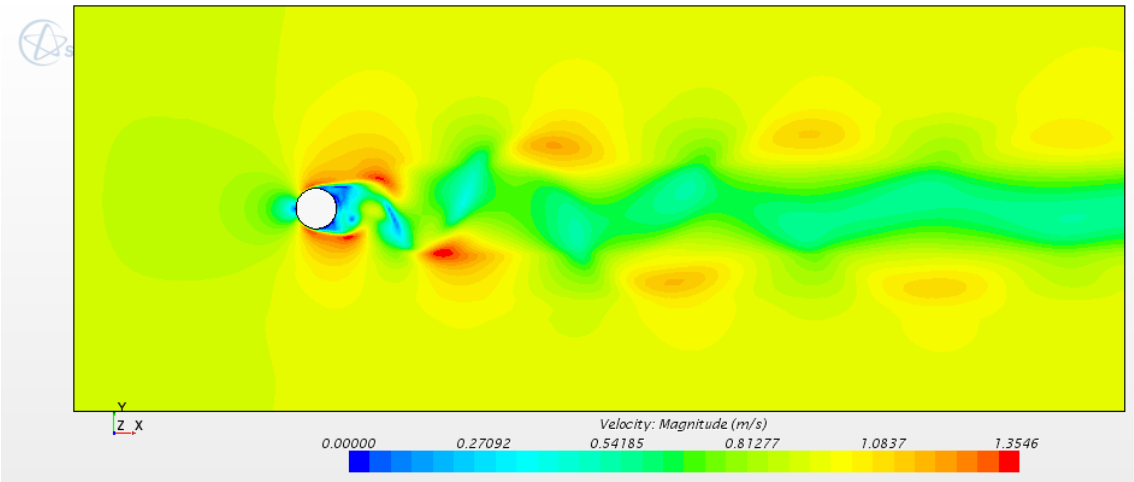

Figure 5.6: Flow separation and velocity distribution for $Re = 1000$

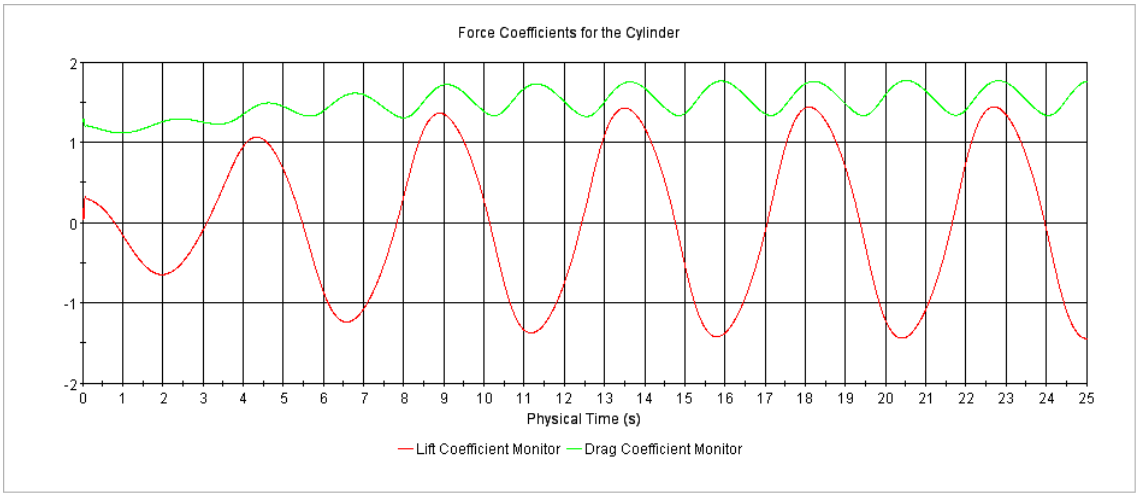

Figure 5.7: Solution history for lift and drag coefficients for $Re = 1000$

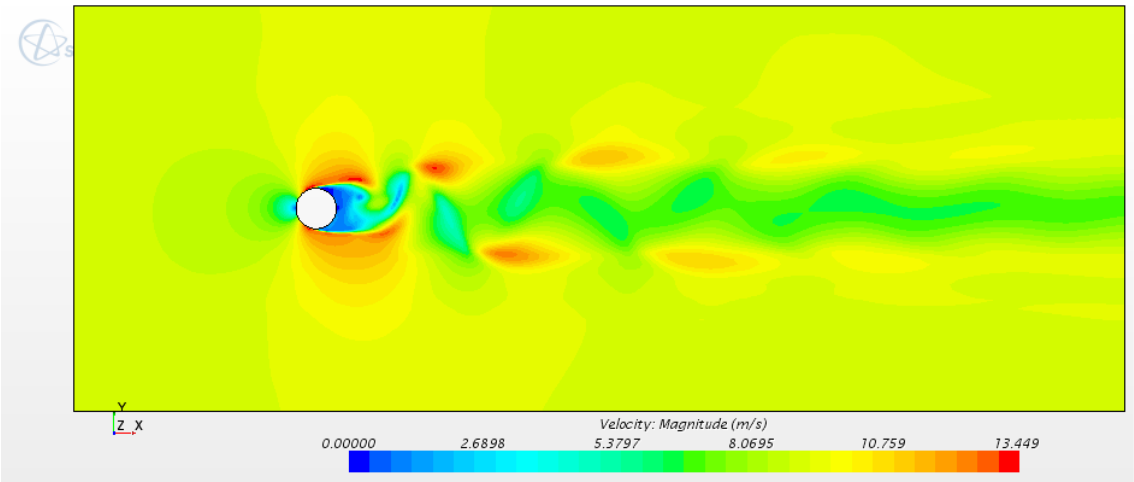

Figure 5.8: Flow separation and velocity distribution for $Re = 10,000$

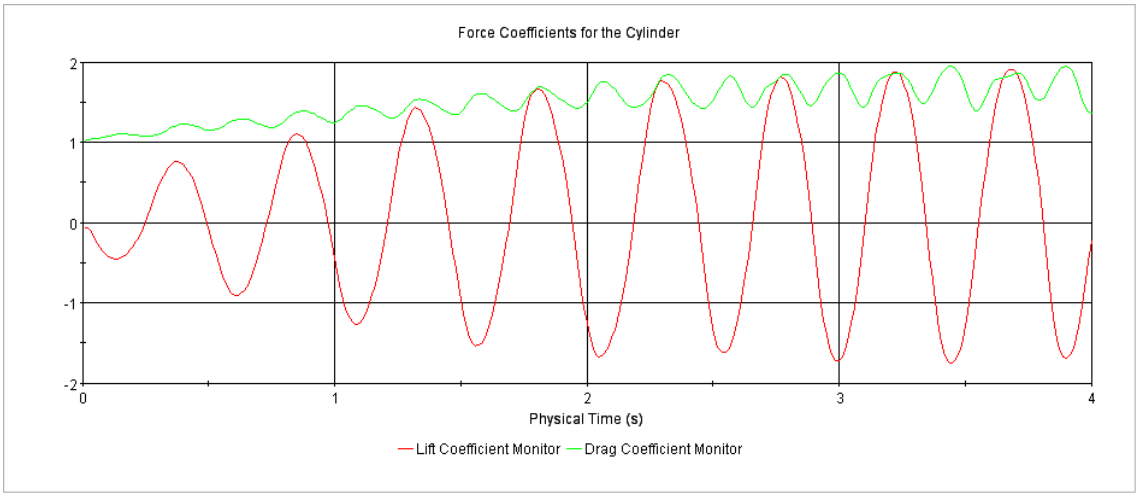

Figure 5.9: Solution history for lift and drag coefficients for $Re = 10,000$

The points at which the vortices detach from the cylinder are dependent on the Reynolds number Re. At a Reynolds number of 100 (see Figure 5.2), the flow is found to separate at a point around 10 degrees upstream of the transverse maximum diameter line. As the Reynolds number increases the point of detachment moves further downstream (See Figure 5.4 & 5.6). At a Reynolds number of $10,000$ (see Figure 5.8), the flow separates from the downstream side of the transverse diameter line [14].

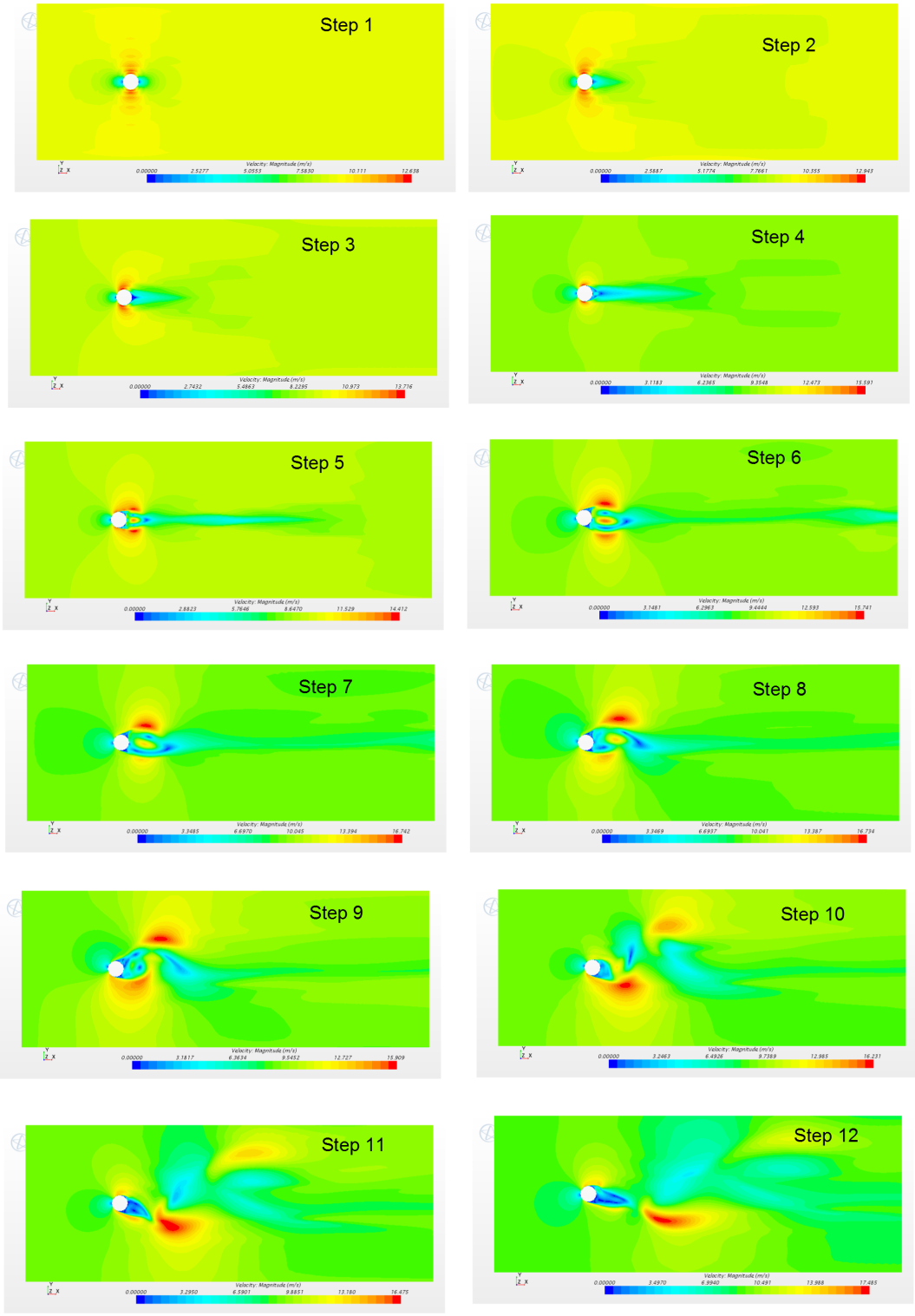

Figure 5.10: Configuration 1: Flow development at $Re = 10,000$

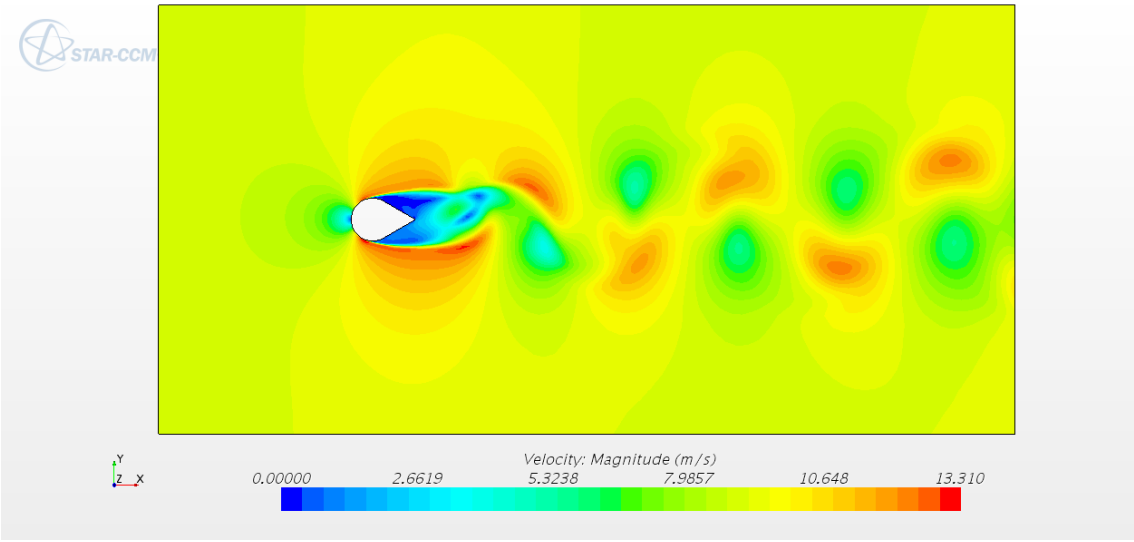

Figure 5.11: Configuration 2: Flow separation and velocity distribution for $Re = 10,000$

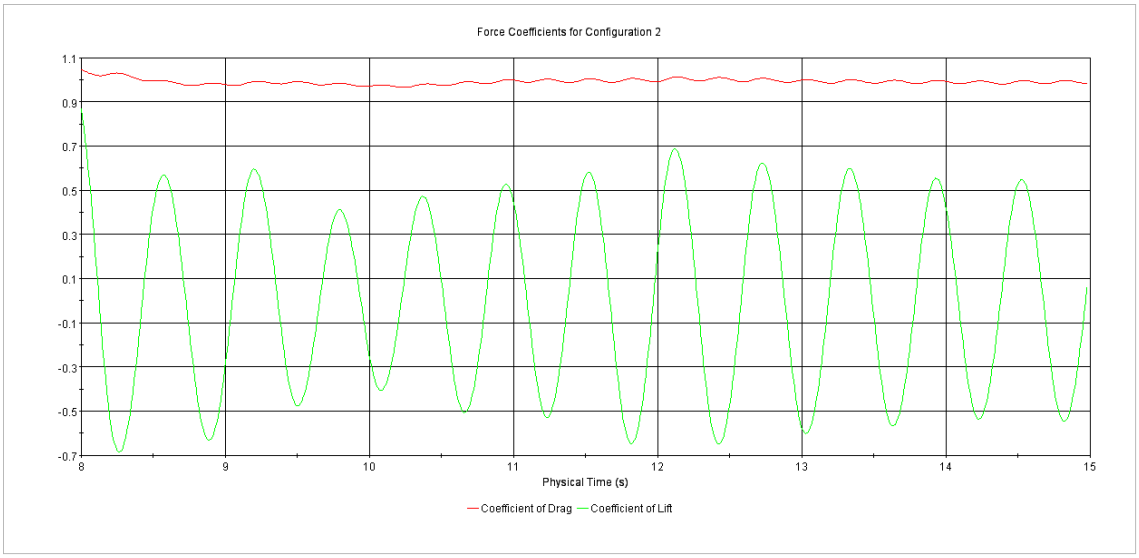

Figure 5.12: Configuration 2: Solution history for lift and drag coefficients for $Re = 10,000$

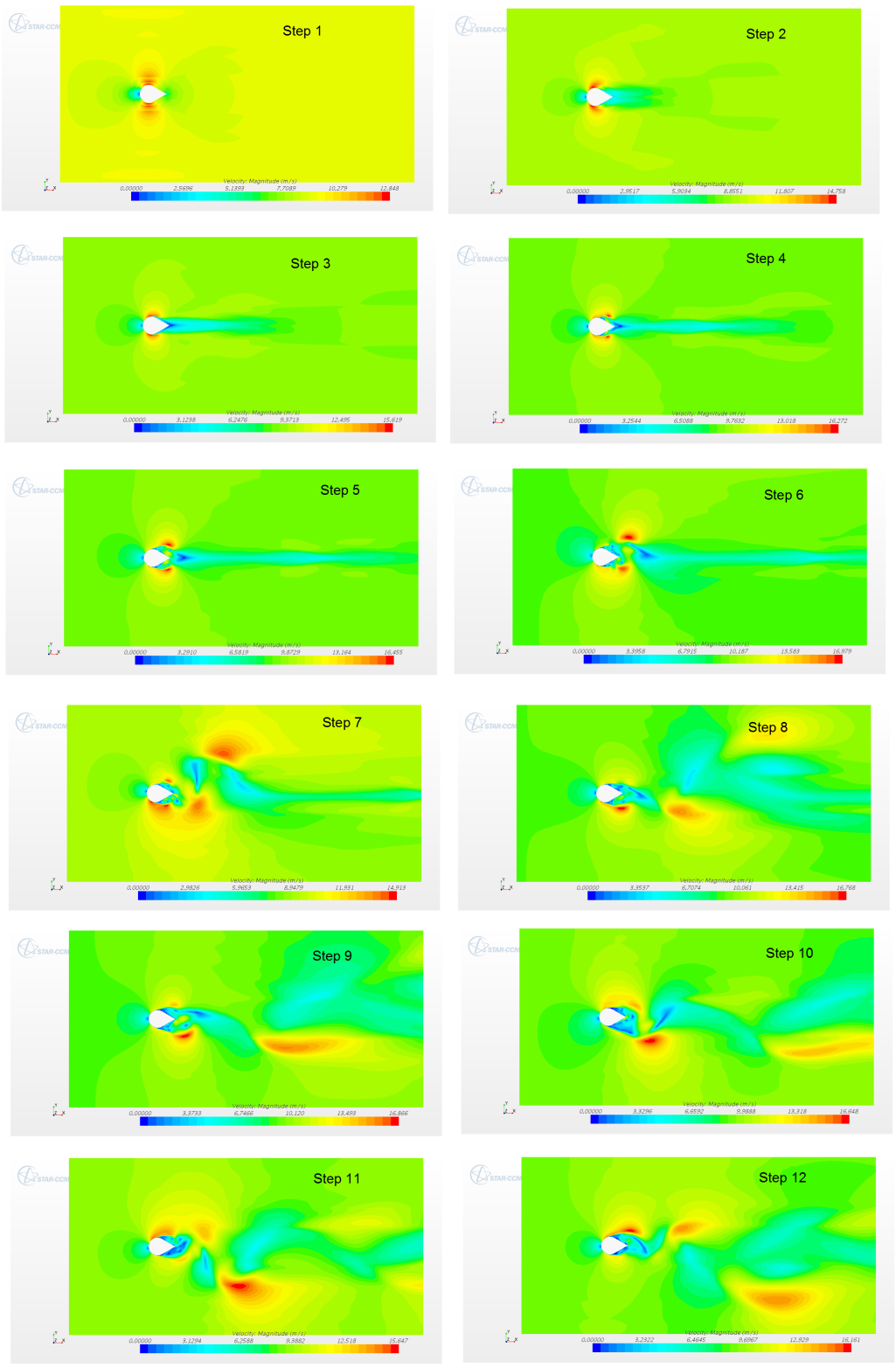

Figure 5.13: Configuration 2: Flow development at $Re = 10,000$

The flow development history of configuration 1 (see Figure 5.10) and configuration 2 (see Figure 5.13) are tabulated above.

5.3.2 Force Coefficient comparison

The force coefficients compared by Asyikin [6] with other scholar works are provided in the Figure 5.14:

Experiment by	Re = 100		Re = 200		Re = 1000	
	Cd	Cl	Cd	Cl	Cd	Cl
Linnick and Fasel [11]	1.34	0.333	1.34	0.69	-	-
Herfjord [9]	1.36	0.34	1.35	0.70	-	-
Berthelsen and Faltinsen [3]	1.38	0.34	1.37	0.70	-	-
Russel and Wang [13]	1.38	0.30	1.29	0.5	-	-
Xu and Wang [17]	1.42	0.34	1.42	0.66	-	-
Calhoun [4]	1.33	0.298	1.17	0.668	-	-
Franke, *et al* [8]	-	-	1.31	0.65	1.47	1.36
Rajani, *et al* [12]	1.335	0.179	1.337	0.424	-	
Present study*	**1.28**	**0.13**	**1.20**	**0.29**	**0.80**	**0.37**
Present study**	**1.42**	**0.38**	**1.29**	**0.48**	**1.40**	**1.22**

** Simulation results for the transient laminar flow*

***Simulation results for the transient turbulent flow (LES model)*

Figure 5.14: Experimental results of the C_L and C_D at Re 100, 200 and 1000 as from Asyikin [6]∗

Please note that the present study mentioned in the Figure 5.14 are from Asyikin [6]

The drag and lift coefficients of the flow computed from the solution histories for Reynolds numbers 100 (Figure 5.3), 500 (Figure 5.5), 1000 (Figure 5.7) and 1.0×10^4 (Figure 5.9) are tabulated in the Table 5.1.

Re	C_L	C_D
100	0.21	1.38
500	1.01	1.27
1000	1.35	1.48
10^4	1.72	1.45

Table 5.1: Lift and Drag coefficients for various Reynolds numbers

Re	C_D from [4] Experimental	C_D from [6] Computational	C_D Present Computation
100	1.80	1.34	1.38
500	1.20	-	1.27
1000	1.01	1.40	1.48
$1.\times10^4$	1.35	-	1.45

Table 5.2: Comparison of drag coefficients

A comparison of the lift and drag force coefficients of the two configurations is also drawn based on the analysis done (see Figure 5.9 & Figure 5.12) at a Reynolds number of $1.0X10^4$:

	C_L	C_D
Configuration 1	1.72	1.45
Configuration 2	0.63	1.01

Table 5.3: Lift and Drag coefficients for the two configurations

There is drastic reduction in the lift and drag coefficient values when the fairing is attached to the bluff body (See Table 5.3).

5.4 Oscillation Amplitude for various Configurations

5.4.1 Oscillation Model Definition

In order to define the oscillating body in a fluid flow motion problem, DFBI case was selected in Star CCM+ (Please see Appendix A for further explanation). Taking into account Gharib's [8] experimental analysis, one linear spring is attached on either side in cross flow direction. One of the models from Gharib's [8] experiment given in Table 5.4 is selected and the mass of the body, spring constant of the springs and structural damping have been adopted accordingly.

Mass (kg)	k (N/m)	Damping Force (N-s/m)
0.545	13.4	0.166

Table 5.4: Mechanical system considered for the analysis [8]

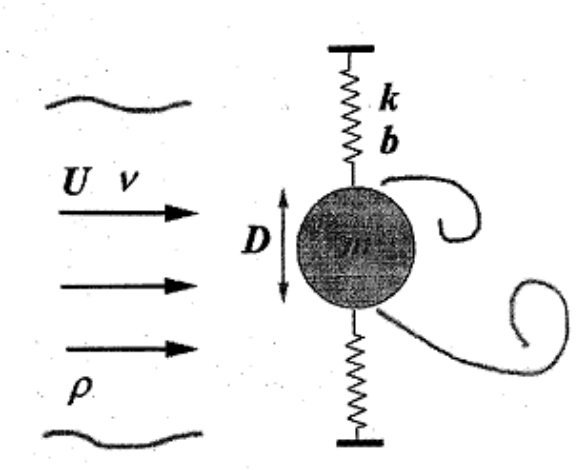

Figure 5.15: Cross-Flow model setup considered for the analysis [8]

To initialize the oscillation, we define the initial center of mass at a position away from the equilibrium position. As the analysis begins, the body is released from the initial position. Otherwise, the analysis will take additional computation time. The mechanical system consisting of mass and spring was tested in the software to check whether the correct natural period (Figure 5.16) and damping effects (Figure 5.17)

are obtained.

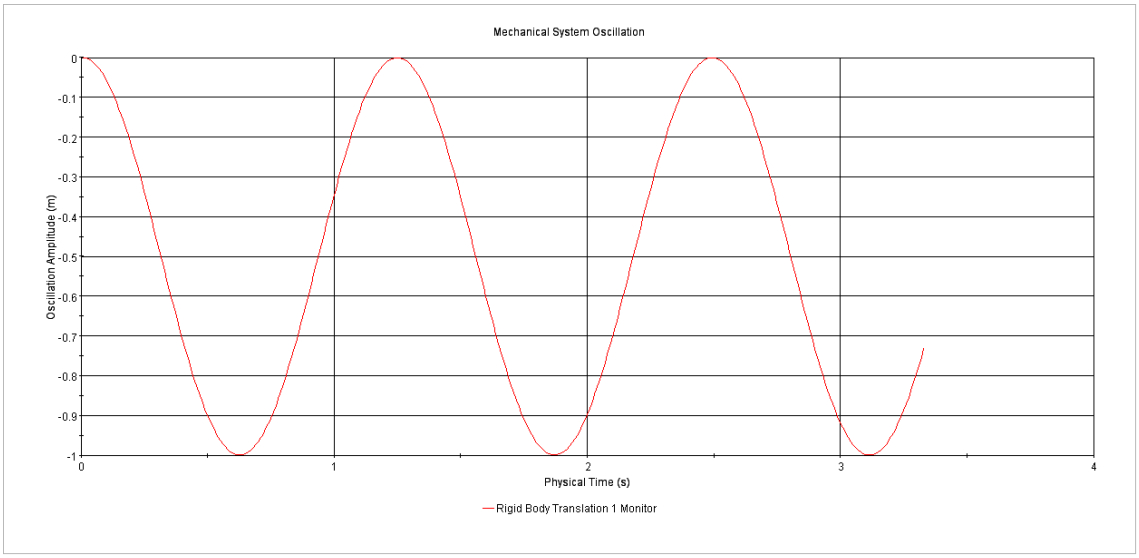

Figure 5.16: Oscillation of mechanical system without any damping

The time period of the system is given by:

$$T = 2\pi\sqrt{\frac{m}{k}} \tag{5.1}$$

With $m = 0.545kg$ and $k = 13.4N/m$, the Time period, $T = 1.267s$. From Figure 5.16, we could see that the time period is coming close to $1.267s$.

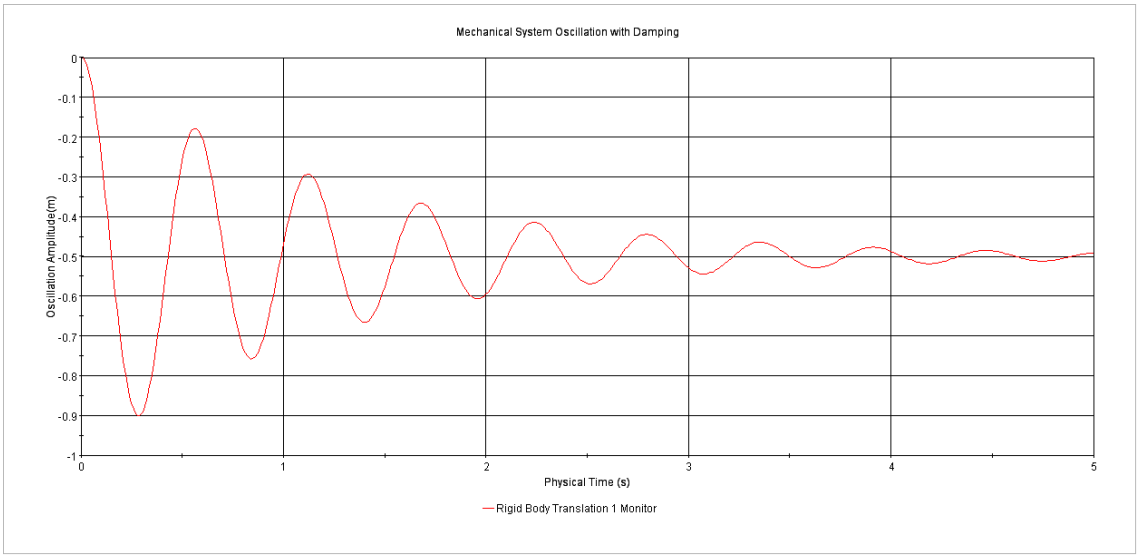

Figure 5.17: Oscillation of mechanical system with structural damping

In addition the oscillation of the body in a fluid at rest is simulated for both the configurations. The results are shown in the figure 5.18 and figure 5.19

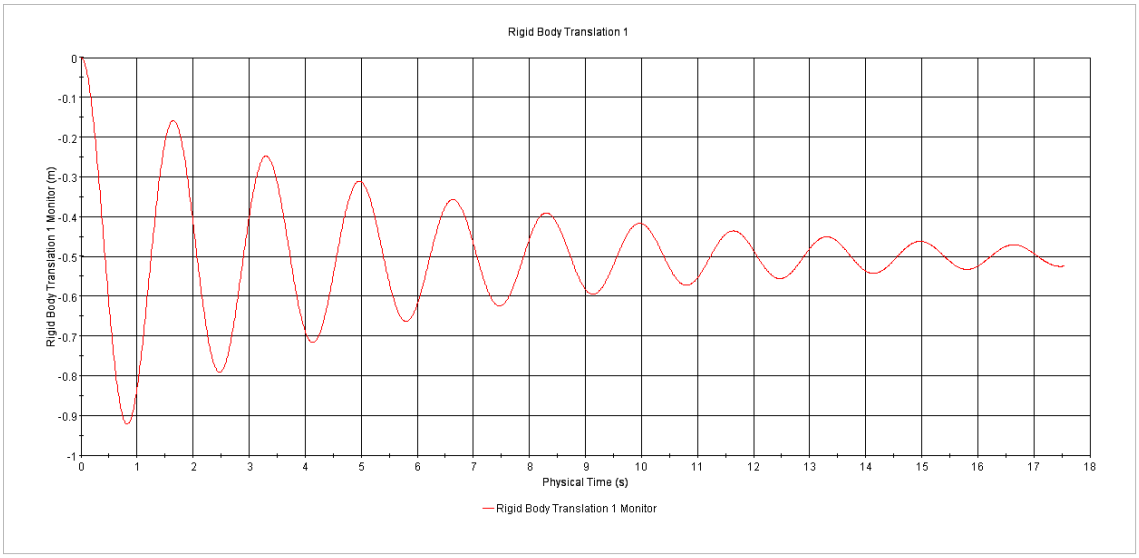

Figure 5.18: Configuration 1: body oscillation in a fluid at rest

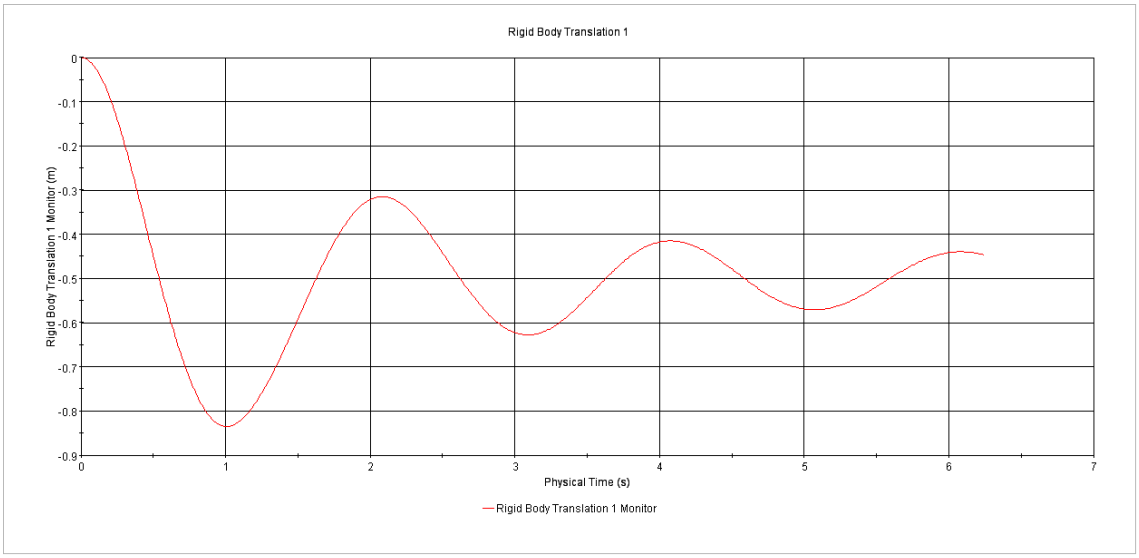

Figure 5.19: Configuration 2: body oscillation in a fluid at rest

When you compare the oscillations for a mechanical system without fluid drag and with fluid drag, decay of the oscillation occurs slower in the system with fluid drag. This is because, cylinder oscillating in transverse direction in a fluid at rest tend to shed vortices in the transverse direction. The force produced acts in the opposite direction of the structural damping. This delays the decay of the body oscillation.

5.4.2 Analysis Outputs

The oscillation history of the cylinders with different configurations are shown below in Figure 5.20 and Figure 5.21. Now the main analysis case, when the oscillating body is placed in a parallel fluid flow is studied. A Reynolds number Re of 1.0×10^4 was selected for this study.

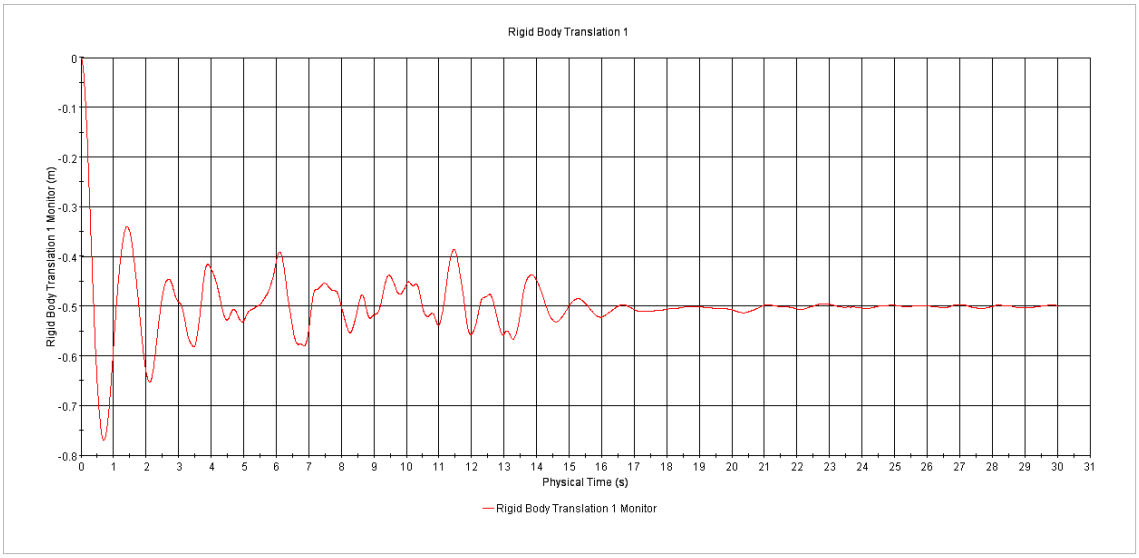

Figure 5.20: Configuration 1: Body oscillation in a constant fluid flow ($Re = 10,000$)

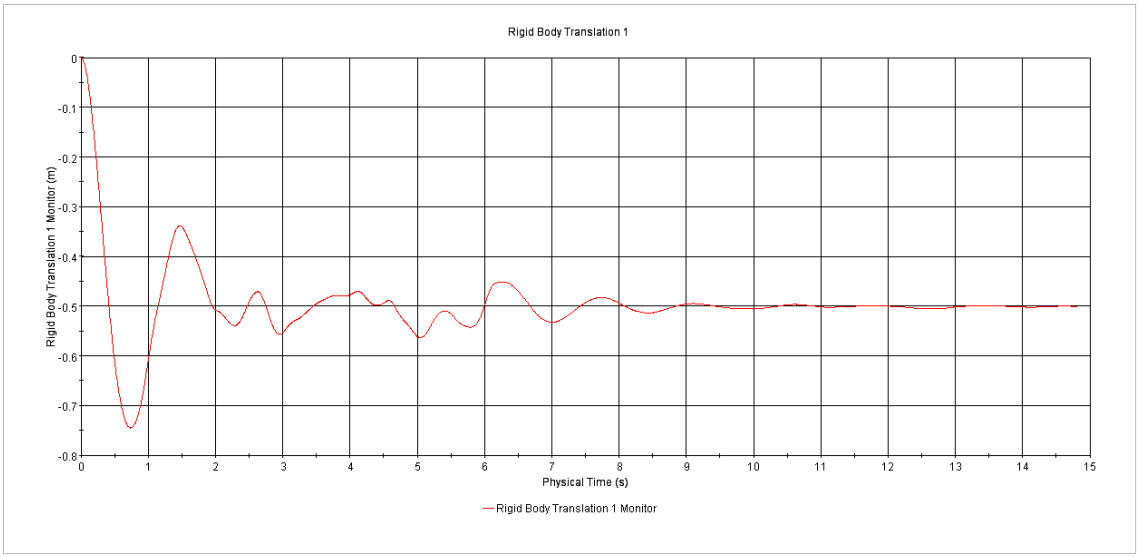

Figure 5.21: Configuration 2: Body oscillation in a constant fluid flow ($Re = 10,000$)

The oscillation start at an initial amplitude of $0.5m$. After some time the initial disturbance has declined and steady state oscillation sets in. Oscillation amplitude are obtained from Figure 5.20 and Figure 5.20 and tabulated in Table 5.5:

	Configuration 1	Configuration 2
Amplitude	5.1 mm	2.7 mm

Table 5.5: Comparison of oscillation amplitude

6 | Conclusions

6.1 Introduction

With all the limitations of the study, author believes the thesis work helped him meet the basic goals of this research work:

- understand the concept of VIV and its dependence on Reynolds number Re
- understand the effectiveness of the fairing in suppressing the VIV of the cylinder

6.2 Conclusion

6.2.1 Bench-Marking

The points at which the vortices detach from the cylinder are dependent on the Reynolds number Re. At a Reynolds number of 100 (see Figure 5.2), the flow is found to separate at a point around 10 degrees upstream of the transverse maximum diameter line. As the Reynolds number increases the point of detachment moves further downstream (See Figure 5.4 & 5.6). At a Reynolds number of $10,000$ (see Figure 5.8), the flow separates from the downstream side of the transverse diameter line [14]. This behavior is studied and confirmed in this thesis work.

The drag coefficients are bench-marked against published experiments and analysis. A comparison of the bench-marking results is provided in the below table:

Re	C_D from [4] Experimental	C_D from [6] Computational	C_D Present Computation
100	1.80	1.34	1.38
500	1.20	-	1.27
1000	1.01	1.40	1.48
$1.\times10^4$	1.35	-	1.45

Table 6.1: Comparison of drag coefficients

It can be noted from Table 6.1 that the drag coefficients are comparable to the experimental values obtained by Asyikin [6].

A comparison of the lift and drag force coefficients of the two configurations is also drawn based on the analysis done at Reynolds number of 1×10^4 :

	C_L	C_D
Configuration 1	1.72	1.45
Configuration 2	0.63	1.01

Table 6.2: Lift and drag coefficients for the two configurations

Based on the Table 6.2, we can conclude that the force coefficients are reduced when the cylinder is attached with a marine fairing.

6.2.2 Oscillation Comparison

The oscillation amplitudes of a regular cylinder and a cylinder with attached fairing are calculated using the program Star CCM+. Tt can noticed that the oscillation amplitude of the cylinder is drastically reduced when a fairing is attached at the downstream end of it.

The oscillation start at an initial amplitude of $0.5m$. After some time the initial disturbance has declined and steady state oscillation sets in:-

	Configuration 1	Configuration 2
Amplitude	5.1 mm	2.7 mm

Table 6.3: Comparison of oscillation amplitude

Comparing the values of steady oscillation of the body (see Table 6.3), we can see a 48% reduction in the oscillation amplitude of the structure. So, it can be concluded that attaching a fairing at the downstream end of the cylinder reduces the oscillation amplitude of the cylinder significantly.
The amount of reduction is somewhat uncertain since the analysis has various limitations which are discussed in the next section.

6.3 Limitations of the Study

The presented analysis of the effect of fairings on the oscillation of marine risers is based on the following assumptions:

- The selected spring model might not simulate the real case scenario as the stiffness of the actual riser might have a different value.
- For the sake of simplicity of the analysis, it was assumed that both configurations have same mass and center of gravity locations. Marine fairings will change the mass and center of gravity.
- The Reynolds number used for the analysis is $Re = 1.0 \times 10^4$. Actual values are usually higher than 1.0×10^6. This might change the results, but it is unlikely to negate the positive effects of marine fairings.
- In this analysis, we considered only the sway motion of the cylinder. All other translatory and rotational motions have been ignored. The sway motion of the cylinder imparts another excitation (MIE), which is called galloping. The present analysis assumes that no galloping occurs. The author considers this a major limitation of the analysis and intends to study this effect in the future.
- Semi 3D models are used for the analysis due to the limitation of the computing facility. In an actual scenario the fluid and structure both must be modeled and the results will be more accurate than the ones presented in the report.
- In a real world scenario water will enter into the small void spaces between the cylinder and the fairing. This will affect the working of the weather vane, which allows the turning of the fairing based on the current heading. So in a way, it will increase drag and oscillation of the body.
- Another major error could arise due to the modeling strategy. RANS equations based turbulence models are easy on the computational side as most of the eddies (both large and small) are modeled and not numerically resolved, but it adversely affects the results. A higher breed of turbulence model like the Detached Eddy Simulation(DES) is available which is likely to produce more realistic results. However, computation times would have increased significally.

6.4 Future Works

The author hopes to continue this study in order to eliminate most of the aforementioned limitations and model the problem in a more accurate manner. More cases of fairings and splitter plates will also be considered for the analysis at a later stage to better understand the VIV suppressing capabilities of different devices.

Bibliography

[1] Lankhorst. Lankhorst VIV fairings. `http://www.lm-offshore.com/en/viv-suppression`, 2014.

[2] E. Naudascher and D. Rockwell. *Flow-induced vibrations âĂŞ- an engineering guide*. IAHR Hydraulic Structures Design Manuals 7. Taylor & Francis, 1994.

[3] R.D. Blevins. *Flow-induced vibration*. Krieger Publishing Company, New York, 2nd edition, 1994.

[4] Y.V. Polezhaev and I.V. Chircov. `http://www.thermopedia.com/content/707/`, 2011.

[5] M.M. Zdravkovich. Review and classification of various aerodynamic and hydrodynamic means for suppressing vortex shedding. *Journal of Wind Engineering and Industrial Aerodynamics*, 7(2):145–189, 1981.

[6] M.T. Asyikin. CFD simulation of vortex induced vibration of a cylindrical structure. Master's thesis, Norwegian University of Science and Technology (NTNU), 2012.

[7] A. Bakker. Computational Fluid Dynamics (ENGS 150). Class notes, Dartmouth College, 2003.

[8] M.R. Gharib. *Vortex-induced vibration, absence of lock-in and fluid force deduction*. PhD thesis, California Institute of Technology, 1999.

[9] R.D. Blevins. *Applied fluid dynamics handbook*. Van Nostrand Reinhold Company, 1984.

[10] T. Sarpkaya. Vortex-induced oscillations: a selective review. *Journal of Applied Mechanics*, 46(2):241–258, June 1979.

[11] C.C. Feng. The measurement of vortex induced effects in flow past stationary and oscillating circular and d-section cylinders. Master's thesis, The University of British Columbia, 1963.

[12] P. Anagnostopoulos. *Flow-induced vibrations in engineering practice*. WIT Press, 1st edition, 2002.

[13] CD-adapco. *Star CCM+ user manual and training manuals*, 2014.

[14] B. Mutlu Sumer and J. Fredsøe. *Hydrodynamics around cylindrical structures.* Advanced Series on Ocean Engineering 12. World Scientific, 1997.

Appendix A :

Modeling the problem in Star CCM+

Introduction

The entire CFD computation was performed using the software Star CCM+, owned by CD-Adapco. This chapter gives an overview of how the thesis problem was setup in Star CCM+.

3-D Modeling

Star CCM+ has a built-in 3D modeling module which can be used to model the entire problem. However the more complex models are usually advisable to be completed in a modeling software and imported into the software. The below figure shows the layout and principal dimensions of the modeled fluid domain.

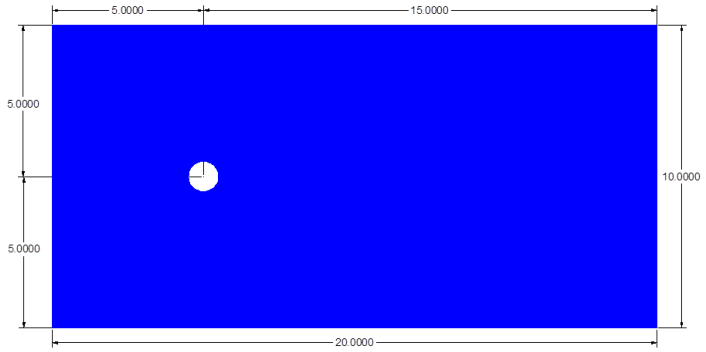

- Create a new 3D CAD model. Once you select a new 3D-CAD Model, the program will take you to the CAD modeler. Since the fluid flow is planar, we create the sketch in the XY plane as shown in the next figure.

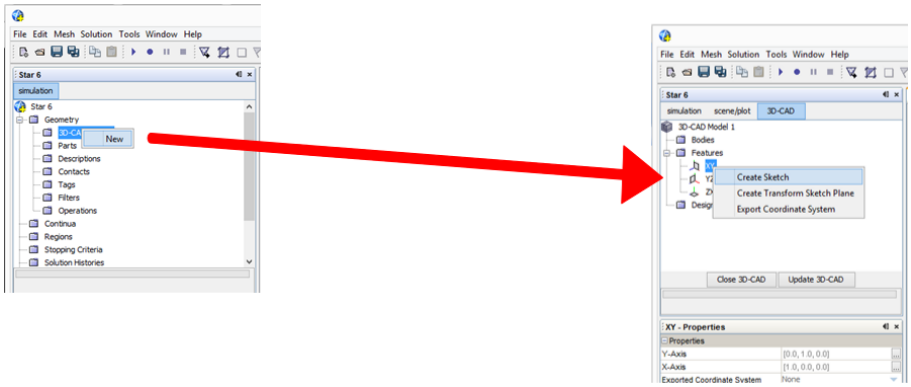

- Once you get into the sketch maker, first select *SetSketchGridSpacing* and set the value to 1.0 m. This is done to ease up the modeling process and has no further implications on the analysis.

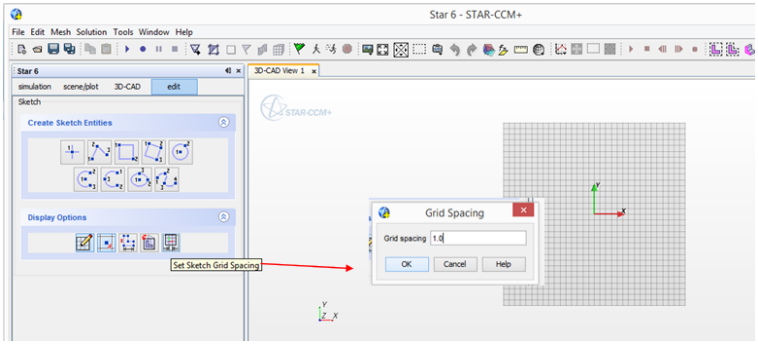

- Now, create a rectangle to define the flow domain we are interested in. Then create a circle to represent the flow boundary due to the presence of the body in the flow.

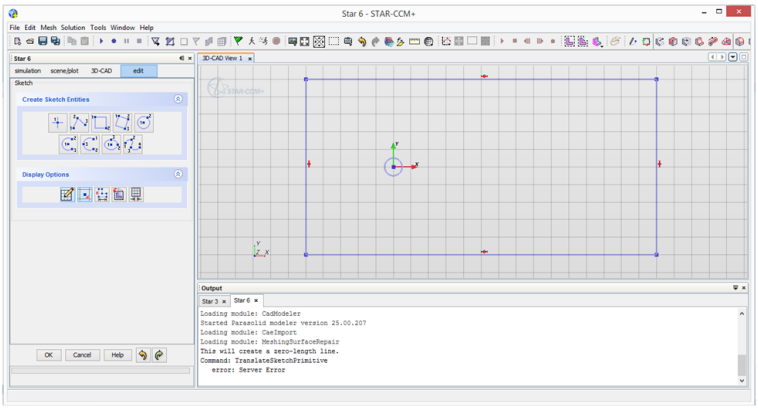

- Left click on the flow boundaries and define *ApplyDimensions* so that we can change the boundary dimensions of the flow domain and the cylinder in the flow at our own convenience at a later stage. Repeat it for all three dimensions defined in our case.

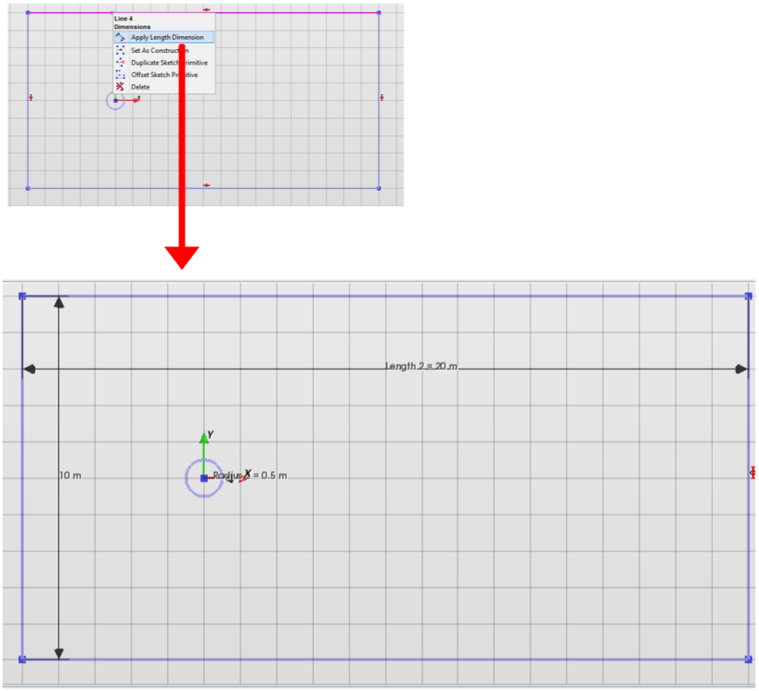

- Now click *OK* and return to the previous window. Since we are interested in the amplitude of the flow, we will have to model the domain as 3D. So, we have to select *CreateExtrude* option to extrude the 2D domain we already created. Define the *Distance* you need to put in ($0.5m$ in our case) and continue.

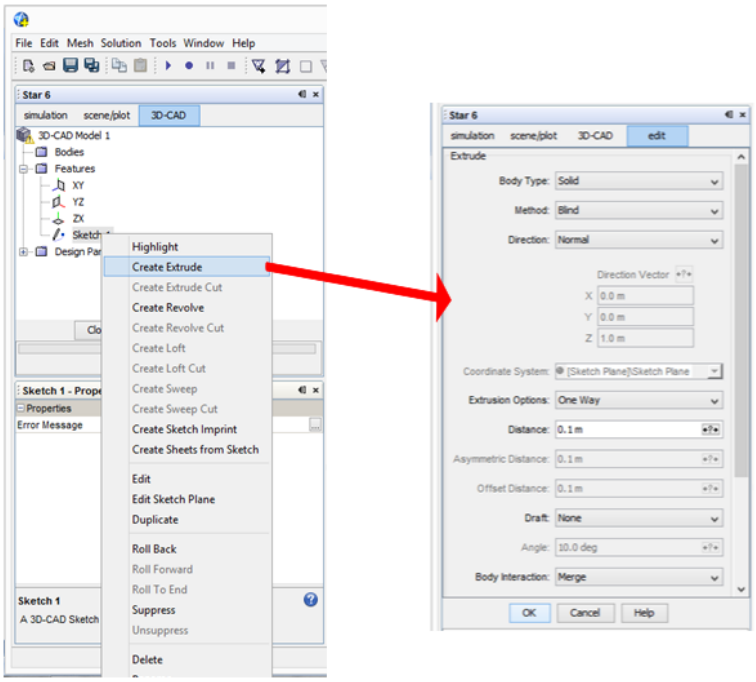

- Once you create the 3D model, it is necessary to rename the boundary faces of the model. This will be helpful for us when we are defining regions. Do it for all the boundary faces of the flow. Once complete renaming the faces, press $Update 3D-CAD$ and then $Close 3D-CAD$. Now your 3D-CAD model is complete.

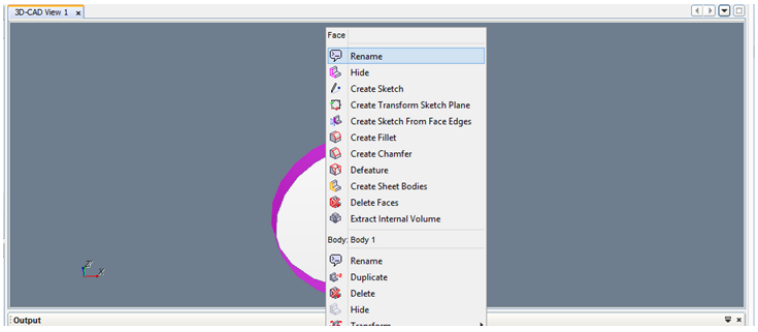

Defining Parts

- Now we need to create a Geometry part from the 3D-CAD model we have created. A part is then allocated to define the solution domain in the problem. Right-click on created $3D-CADmodel1$ and select $NewGeometryParts$.

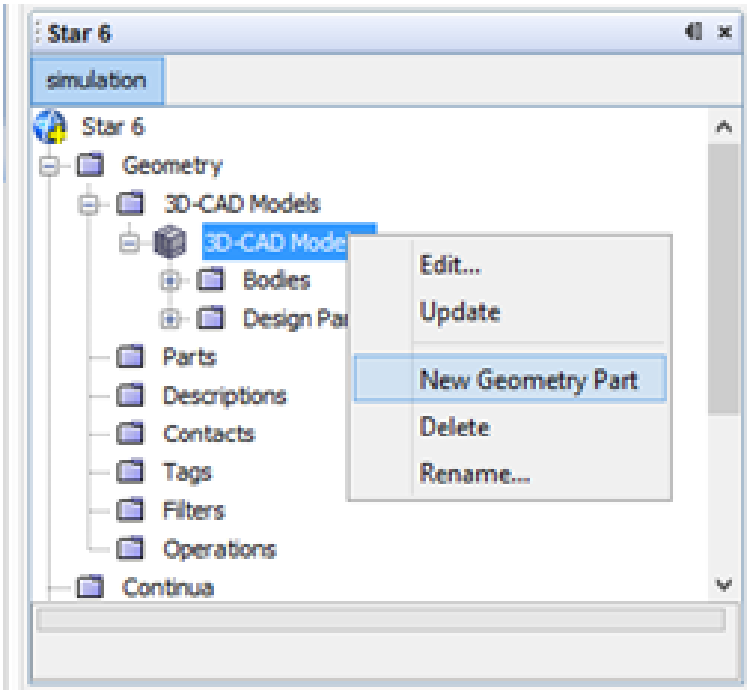

- It is unnecessary to provide a fine meshes at the far-field boundaries. For the location of the body in the fluid, we have to define a mesh which is finer at the cylinder and its wake but more coarse towards the boundaries. For that, we define a *NewShapePart* as *Block*. Follow the figure below to follow the defining of the new block.

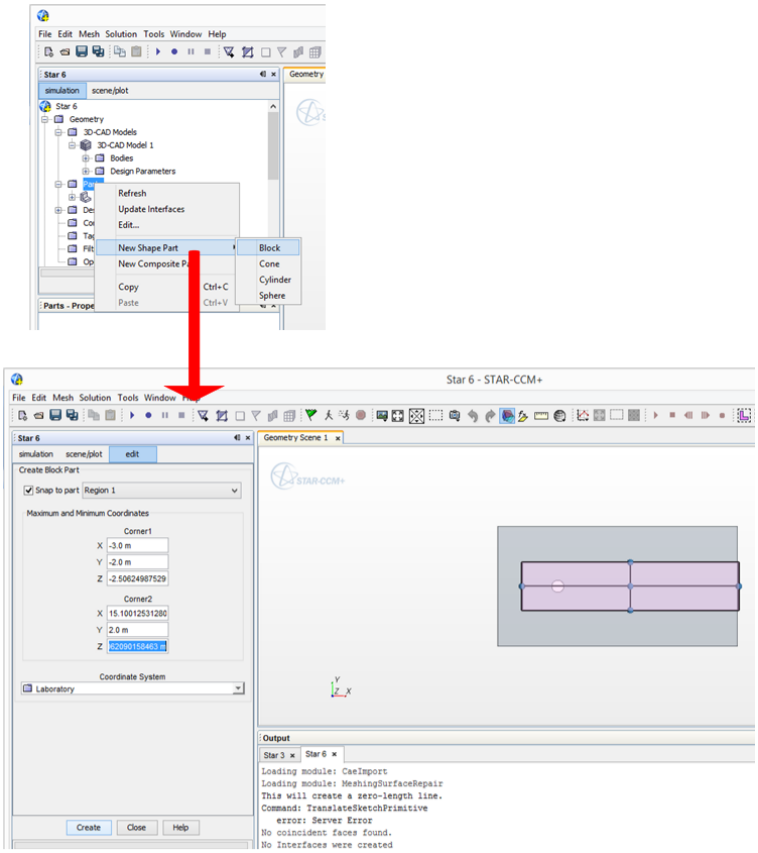

Region

Once we create the geometry part, we now have to create a flow region based on it.

For that we use the command *AssignPartstoRegions*.

Since it is necessary to define the boundaries for the flow, we have to select $OneBoundaryperPartSurface$ from the Boundary mode pull-down menu. Once all options are selected, press *CreateRegion*

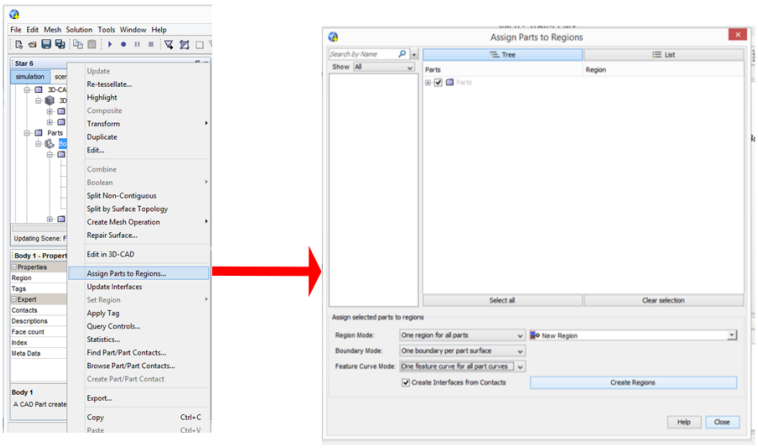

Meshing

- Now under *Operations*, select *NewAutomatedMesh*. Select the *Body*1 from the list, *PrismLayerMesher*, *TrimmedCellMesher* , and *SurfaceRemesher*. We define the mesh as structured and prismatic by *PrismLayerMesher* option, cut the geometry for fine meshes by opting *TrimmedCellMesher*, and remesh the initial surface to provide a quality discretized mesh that is suitable for CFD by opting *SurfaceRemesher*.

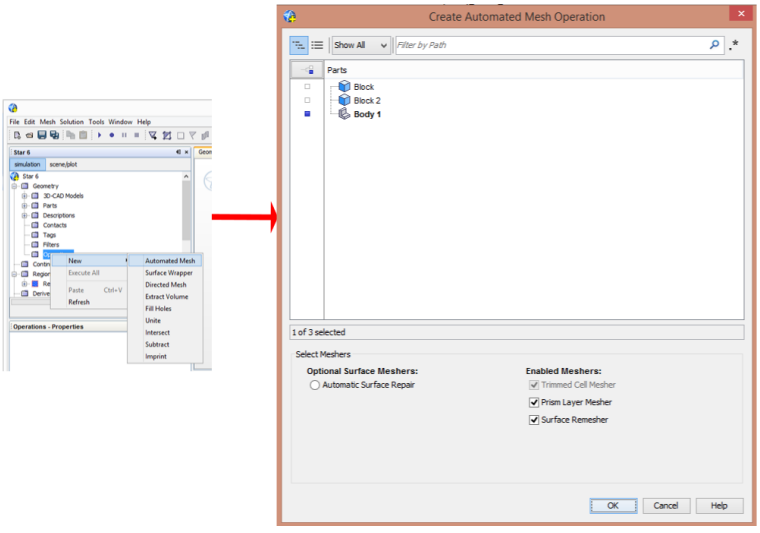

- In the *Default* tab under the Automated mesh, select the following
  Base Size of mesh = 1.0 m
  Target Surface Size = 50.0 percentage of base

Minimum Surface Size = 50.0 percentage of base
Number of Prism Layers = 10
Volume Growth = Very Slow

- In the $CustomControl$ menu under $AutomatedMesh$, we define the mesh refinement. Right-click on $CustomControlMenu$ and select the surface control and volumetric control
  - Prism Surface Control Condition - The body boundary requires prism layers. This must be defined using a surface control condition
  - No Prism Surface Control Condition - Except for the body boundary condition, all the other boundary conditions do not require prism layers. This is because we are more concerned with the body boundary and the far field conditions are not a part of the scope of the thesis.
  - Wake Volumetric Control - We have to define the mesh in such a way to reduce the computation time. Remember, we defined two $Block$s to make the mesh finer at the location of interest, one to capture the wake and the other in vertical direction to capture transverse oscillation. We will define $TrimmerCustomizedsize$ for the volumetric control 10 percentage of the base size.

The meshed domains for configuration 1 (upper) & configuration 2 (lower) will look like as given below:

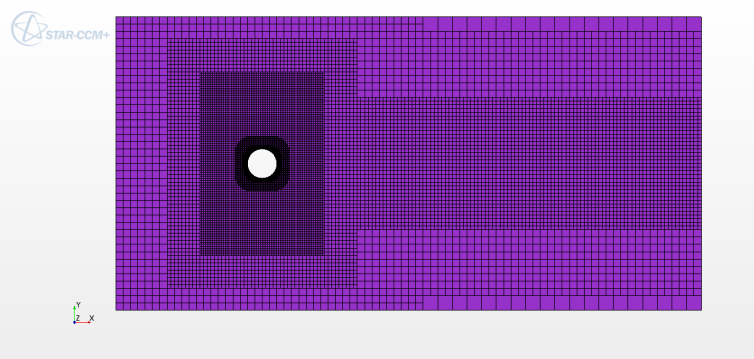

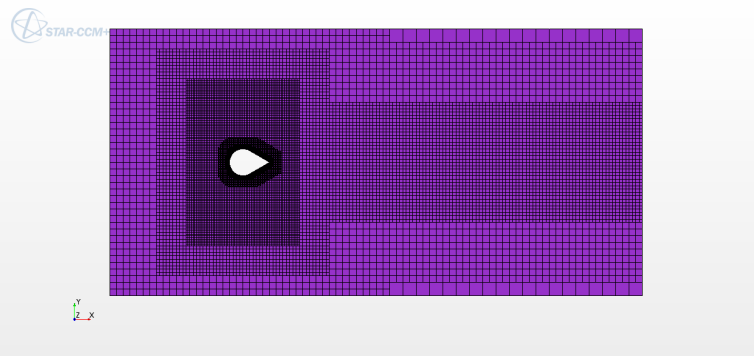

Physics Modeling

Our Problem is a 3D turbulent, segregated liquid flow problem. We use a k-ϵ model, with a constant density. We setup the problem in implicit unsteady time model solver. Implicit unsteady time model is the only unsteady model available with the segregated flow problems. We define the density of the fluid as $1.0kg/m^3$, kinematic viscosity as $8.9 * 10^-4$. The initial velocity is provided as $8.9m/s$.

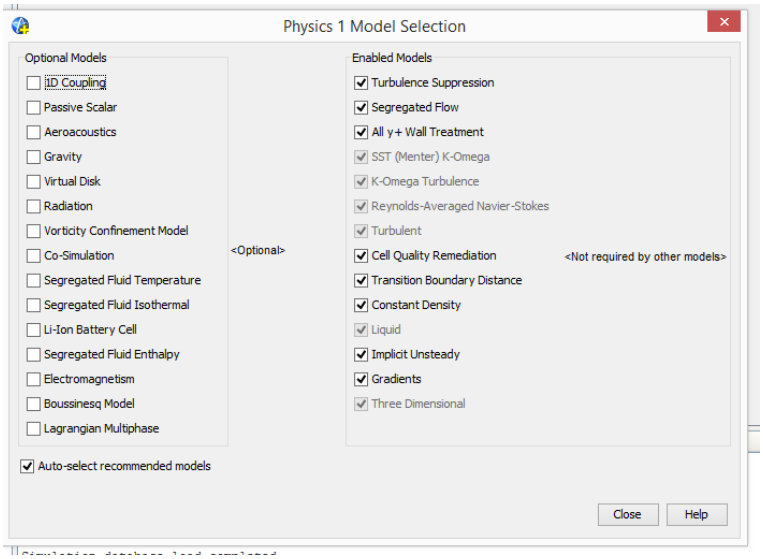

Boundary Conditions

Previously we defined the part surfaces. Once the region is defined and the mesh has been assigned to it, we need to define the boundary conditions for the flow.

- inlet surface is defined as velocity inlet and an inlet velocity is defined to show

the flow direction.

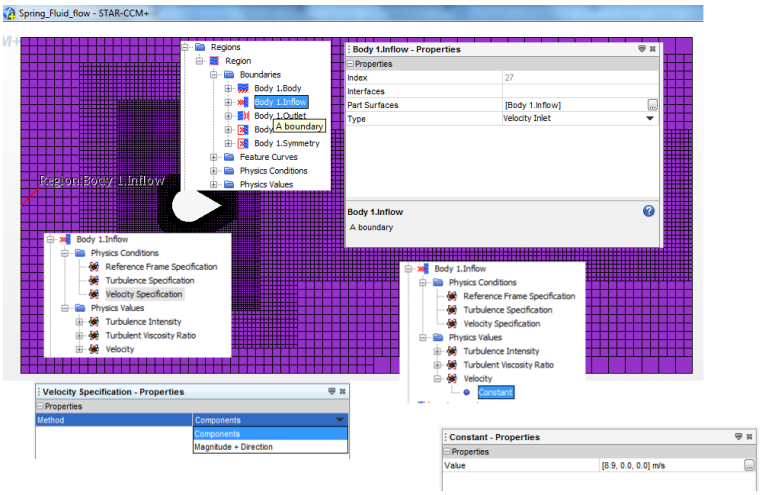

- outlet surface is defined as pressure outlet and the absolute pressure is defined.

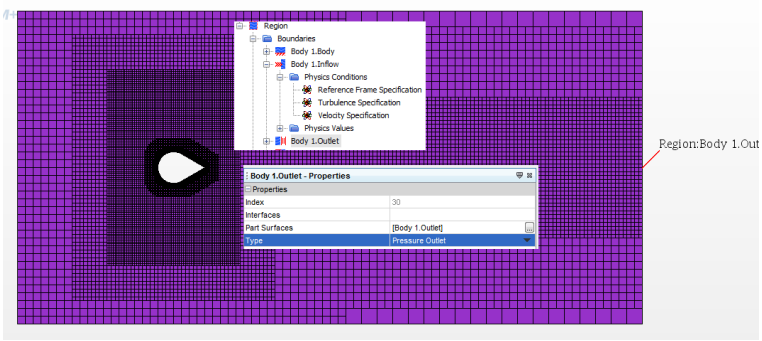

- body surface is defined as a no-slip wall to restrict the flow across the body boundary. There will be a tangential component of shear stress towards the domain.

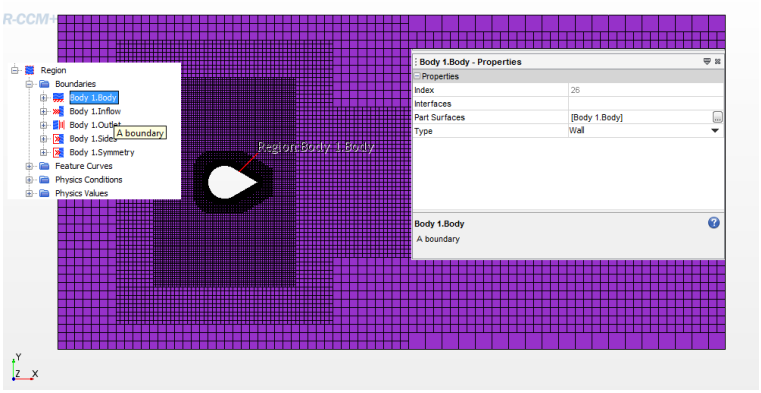

- Sides, Top and Bottom are defined as Stagnation Inlet, which means there is no inward flow through that boundary.

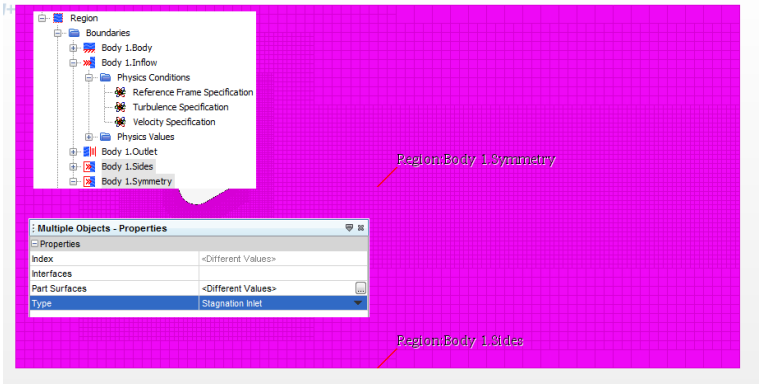

DFBI definition

DFBI is dynamic fluid body interaction module used to simulate the motion of a rigid body in response to pressure and shear forces the fluid exerts, to additional forces we define.

- To describe the motion response of a body, we have to model the body in a DFBI system. Go to *Motions* under the *Tools* tab and select $DFBIRotation\&Translation$

- Now we have to give the motion specification for our body as a DFBI case. For this, we go $MotionSpecification$ under *Regions* and select $DFBIRotation\&Translation$

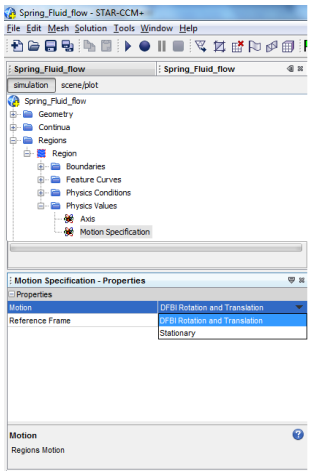

- We can see a new tab "DFBI". A new body is already defined under the tab. Input the mass of the body and Select $FreeMotion$.

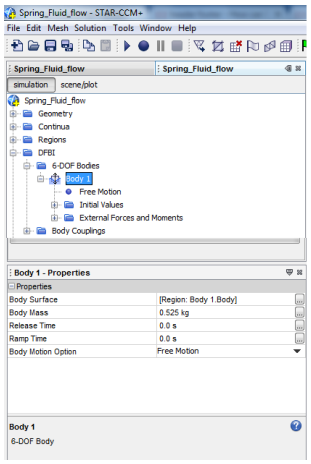

- In the problem we are looking at, we are considering only the sway motion, i.e. translation in Y-direction. Check only $Y - Translation$

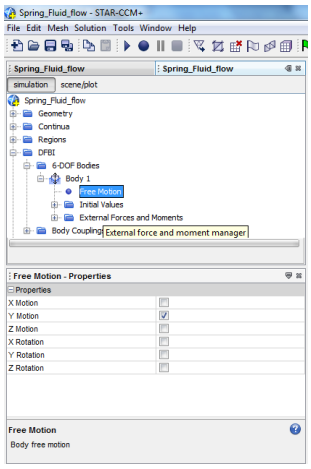

- We define one linear spring on each side of the body, to simulate a forced oscillation. Both of the spring must of same stiffness.

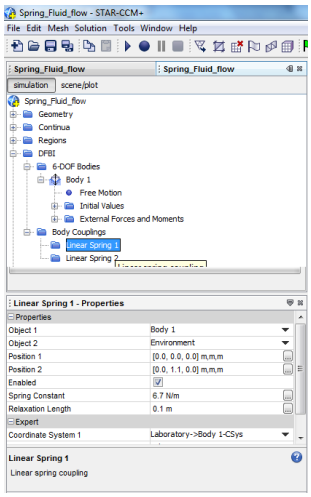

- Define the structural damping of the body. Right-click on $External Forces and Moments$ and select $Damping Force$ from the pull-down. Now click on the $Damping Force$ and below at the properties, input the damping constant.

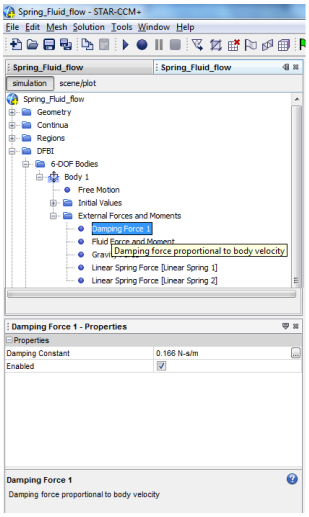

- In order for the motion to start we define an initial position for the center of gravity of the body from where it will be released once the flow starts.

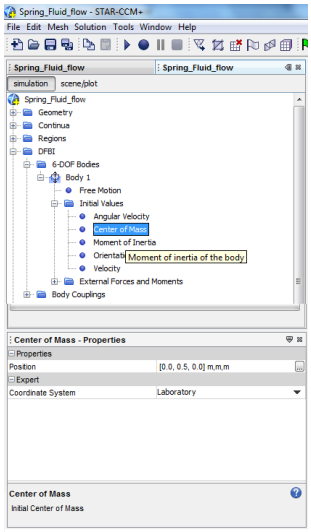

Solvers

- Implicit Unsteady - We define the time step as 0.005s and second order temporal discretization. The time step remains constant based on the user input.

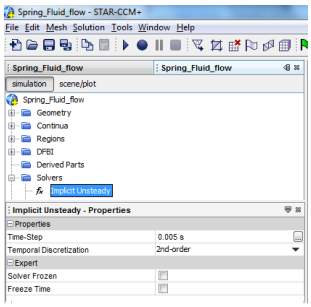

- 6-DOF Solver - We define the maximum number of iterations to 15 for each time step.

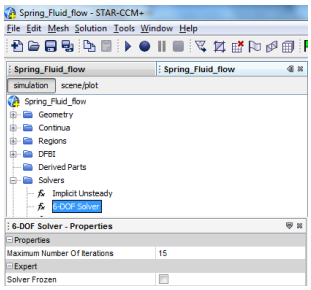

Stopping Criteria

- Maximum number of inner iterations - We have to select it in such a way that it should be twice the value of 6-DOF solver iterations we have already selected in the solver. So we select 30 inner iteration per time step for the analysis.

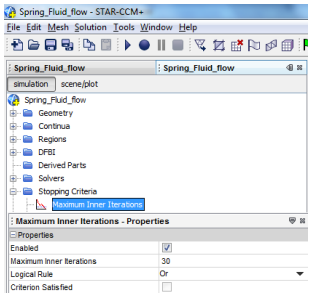

- Maximum physical time - Select the physical time of the analysis you are looking ahead for. Usually that spans from 20s to 40s, depending upon your focus of interest.

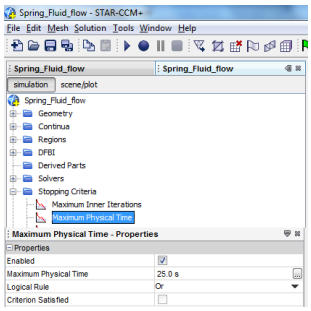

Solution Report

- Select the new report based on what you are interested in from the list as shown below

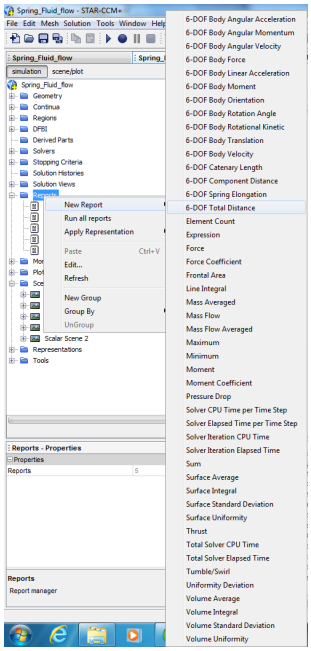

- Select the direction of the quantity you are looking at. For example, for the drag coefficient, the direction is the X-axis (1.0, 0.0, 0.0). Similarly for lift coefficient (0.0, 1.0, 0.0).

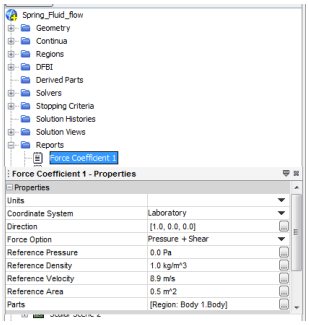

- Right click on the report you have created and click on *CreateMonitorandPlot*. Then a plot will appear below.

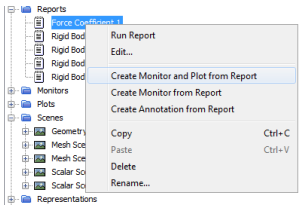

Solution History & Monitoring

- First right-click on the *solutionhistory* tab and select *New* and name it.

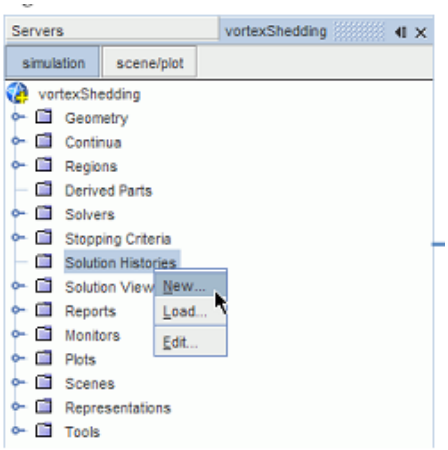

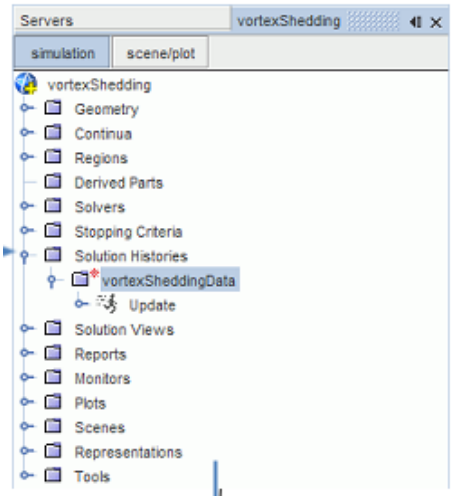

- Select the *Scalar* and *Vector* quantities of which you are interested to store the solution history.

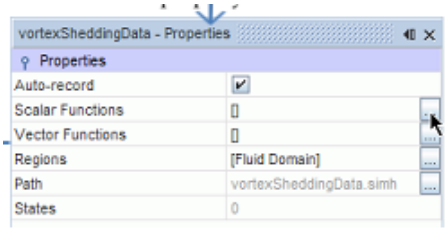

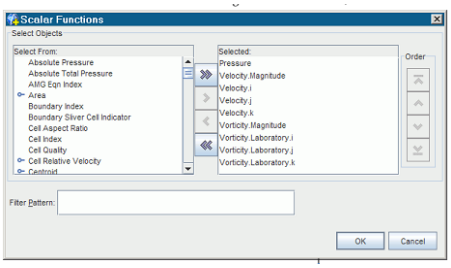

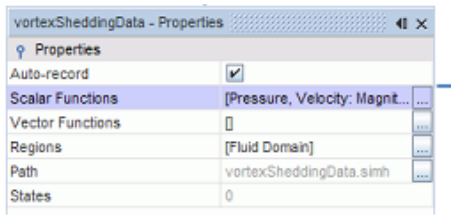

- Click on *Update* and select the *UpdatePolicy* as *Timestep*

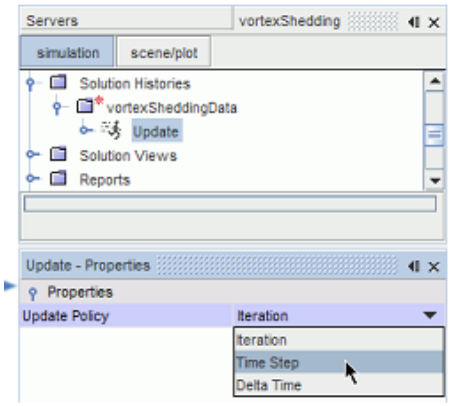

Once all is completed, you click *Solutions*. From the pull-down menu, you first *Initialize* the flow and the *Run* the analysis.

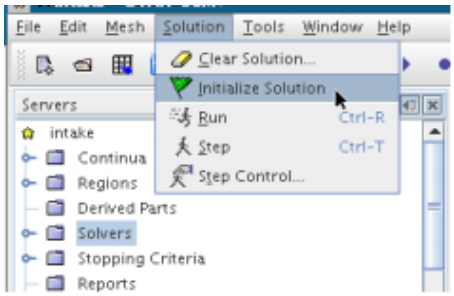

VITA

Aswin Janardhanan (Buddhan) was born in Palghat, India, the son of Sheena Kunjunni Babu and Kottathara Janardhanan. He did his schooling at Kendriya Vidylaya Malappuram, India. He completed his undergraduate degree from the most prestigious Naval Architecture School in India, Cochin University of Science & Technology. He then worked in India and Middle East as Naval Architect, supporting Offshore Oil & Gas industry over a span of five years. He was enrolled in University of New Orleans to attain his MS in Naval Architecture & Marine Engineering in Fall 2012. He is a passionate dreamer, and he aspires to contribute his best as a Naval Architect for the betterment of the society.

The thesis report was entirely typed by the author.